FinEstBeAMS beamline review report

The FinEstBeAMS beamline team

September 2022

Contents

1. Introduction

FinEstBeAMS – Finnish-Estonian Beamline for Atmospheric and Materials Sciences – is a multipurpose beamline at the 1.5 GeV storage ring at MAX IV Laboratory. The beamline has mainly been funded by Finnish and Estonian contributions to the MAX IV Laboratory (see Section 1.1 for more details). FinEstBeAMS is a part of MAX IV beamline portfolio and access policies serving researchers world-widely. The technical specifications of FinEstBeAMS and the selection of research directions reflects the interests of the Nordic-Baltic collaborations rooting to MAX-lab, the predecessor of MAX IV. The FinEstBeAMS is designed to enable research in gas-phase electron and ion spectroscopy, photoluminescence spectroscopy of inorganic materials, and surface science under ultra-high vacuum conditions. In particular, FinEstBeaMS has a unique role globally in Low Density Matter and photoluminescence research.

FinEstBeAMS receives synchrotron radiation from an elliptically polarizing undulator (EPU) and monocromatizes it with a plane grating monochromator using collimated light (cPGM). The operation range of the beamline is exceptionally large: it covers photon energies 4.5 - 1300 eV or, expressed in words, it extends from ultraviolet (UV) to soft X-rays. Another defining characteristic of FinEstBeAMS is that the EPU can deliver linearly polarized radiation in different directions (horizontal, vertical, inclined) as well as left- and right-circularly polarized radiation. Horizontal and, to lesser extent, vertical polarizations have been used in experiments. The development of other polarizations is under progress. The technical specifications and performance of the beamline are described in detail in Section 2.

FinEstBeAMS has three dedicated end stations that are or can be installed at two branch lines: a gas-phase end station (GPES), a photoluminescence end station (PLES), and a solid-state end station (SSES). The GPES was designed for coincidence measurements between energy-resolved electrons and ions, but it can also be used for stand-alone electron spectroscopy and ion time-of-flight (TOF) spectroscopy. The PLES is used in optical spectroscopy to collect emission spectra in the wavelength range 200-1350 nm and excitation spectra in the operation range of the beamline, while allowing the temperature of samples to be varied from 10 K to 300 K. The GPES and PLES nowadays share one of the branches (Branch A); however, when the PLES is not used in experiments, it is dismounted from the beamline. The SSES is a newer end station, which, due to its complexity, is permanently installed at the other branch (Branch B). It was designed as a high-throughput apparatus for X-ray photoelectron spectroscopy (XPS), angle-resolves photoemission spectroscopy (ARPES) and X-ray absorption spectroscopy (XAS). The three end stations are presented in this report in Sections 3-5. Readers should bear in mind that the SSES is still developing; it has not yet fully reached its planned baseline capabilities.

Section 6 contains information about the operation of FinEstBeAMS, including statistics about proposals submitted to FinEstBeAMS, use of beamtime, users, and publications. In addition, present beamline staff are introduced and a description of workflow is given. FinEstBeAMS began regular user operation as the fourth beamline at MAX IV in April 2019. Both the GPES and the PLES have been in user operation since then. The SSES has properly been in user operation only this year (2022), neglecting an outlier beamtime during the pandemic in summer 2021. The scientific output of FinEstBeAMS therefore almost exclusively results from experiments performed at the GPES and PLES. During the period under review (2019-2022), user operation at MAX IV suffered a lot from the Covid-19 pandemic. At FinEstBeAMS, all user beamtimes were cancelled from 16 March to 6 July 2020, and FinEstBeAMS was completely closed from 18 January 2021 until the last week of May 2021. The FinEstBeAMS staff worked remotely during the shutdown. MAX IV was reopened to external users in September 2021, but most users coming from outside European Union were still blocked by local travel

bans. The effects of the pandemic will no doubt be felt over several years as a reduced number of publications.
In Section 7, research performed at FinEstBeAMS is described. Two of our frequent external users, Prof. Edwin Kukk (University of Turku, Finland) and Prof. Marco Kirm (University of Tartu, Estonia), report of their studies in gas-phase spectroscopy and photoluminescence spectroscopy, respectively. Two examples of in-house commissioning and in-house research, performed by the members of the FinEstBeAMS team and collaborators, are also included.
Although FinEstBeAMS has been in user operation for more than three years, the development of the beamline and its end station has continued all the time. Understandably, that part of beamline activities greatly slowed down during the Covid-19 pandemic and sometimes even halted completely, as MAX IV staff were not allowed to work on site. Some known problems and their solutions related to the end stations are addressed within Sections 3-5. Presently, a particular focus point is to bring the SSES to its full baseline capability. On-going and planned development projects affecting the whole beamline are described in Section 8.

1.1. Funding

When regular user operation began in 2019, the total construction costs of the FinEstBeAMS beamline and its end stations had reached 7.0 M€. Finland's share of funding was 3.5 M€ and it came mostly from the Academy of Finland through Finnish Research Infrastructure funding that had been awarded to the University of Oulu, the University of Turku, and Tampere University. In addition, Finland had committed to pay 0.7 M€ for the operation costs of MAX IV Laboratory. Estonia's contribution to the construction of FinEstBeAMS amounted to 3.0 M€, consisting of a 2.5 M€ grant from the European Regional Development Fund of the European Union and an additional funding of 0.5 M€ from the University of Tartu. The contribution of MAX IV Laboratory to the infrastructure of FinEstBeAMS was 0.5 M€. Prof. Marko Huttula (University of Oulu) has acted as the coordinator of the FinEstBeAMS beamline project.
Nowadays, the operation of FinEstBeAMS is funded by the operation budget from MAX IV Laboratory, similarly to most MAX IV beamlines. One part of the annual budget is the running cost budget, which for FinEstBeAMS has been in the range of 600-700 kSEK (60-70 k€) for the last three years (2020-2022). This amount includes the costs for service and maintenance of instrumentation. In addition, FinEstBeAMS has obtained so-called upkeep funding from MAX IV for some small or medium-size investments that cannot be covered by the running cost budget. These are typically in the order of 200 kSEK (~20 k€) per project, but the most expensive one, which aims at the installation of a chopper at FinEstBeAMS, received a partial funding of 750 kSEK (~75 k€) through the upkeep process.
The Estonian and Finnish partner universities of FinEstBeAMS have continued to support the beamline financially and instrumentally after the beginning of regular user operation. They have also sent guest researchers to work at the FinEstBeAMS beamline for extended periods.

2. FinEstBeAMS beamline

2.1. Technical description

2.1.1. Overview of the beamline design

The optical layout of the FinEstBeAMS is shown in Fig. 2.1.

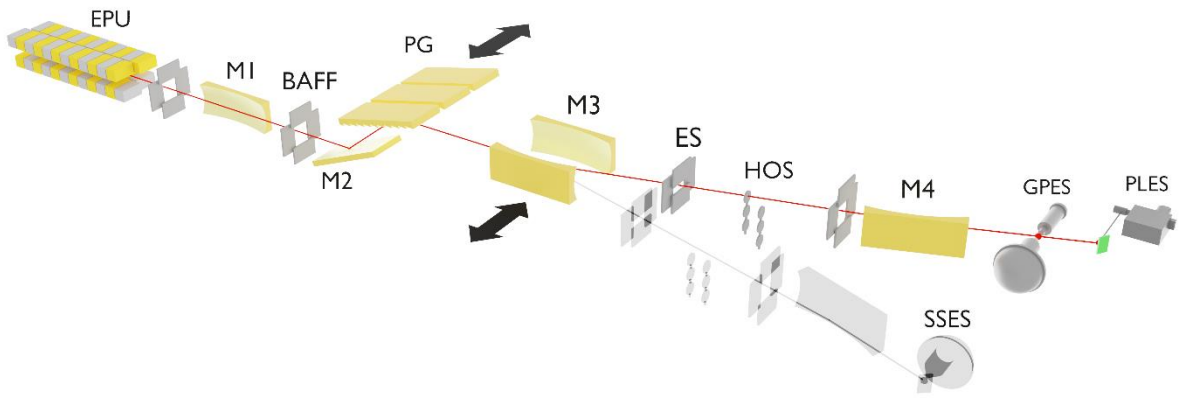

Figure 2.1. *Schematic layout of the beamline's optical system. The following abbreviations are used: EPU – elliptically polarizing undulator, M1–M4 – mirrors, BAFF – baffles, PG – plane grating, ES – exit slit, HOS – higher order suppressing filters, GPES – gas-phase end station, PLES – photoluminescence end station, and SSES – solid state end station.*

The photon source, the elliptically polarized undulator (EPU) of the APPLE II type, was built in-house based on the design used at Helmholtz-Zentrum Berlin (HZB). It has a very long magnetic period, 95.2 mm, to produce effectively photons in the ultraviolet spectral region at the 1.5 GeV storage ring. The undulator contains four arrays of magnets that can be shifted independently in the longitudinal direction, allowing the full control of polarization of radiation. The EPU control system has been commissioned to operate in two modes: helical and inclined. In the inclined mode, two diagonal arrays of magnets move antiparallel, producing radiation with a zero phase shift between the horizontal and vertical components of the electric field vector. In the helical mode, the arrays of the magnets move parallel, resulting in a phase shift of $\pi/2$. The magnitude of the magnets' shift changes the ratio between the vertical and horizontal components of the electric field vector. In the inclined mode, it allows us to obtain linearly polarized light with a chosen angle of inclination. In the helical mode, it is possible to obtain circularly polarized light by equalizing both components of the electric field vector. Linear horizontal and vertical polarizations can be produced in both modes by having the shift equal to zero or half of the magnetic period (47.6 mm), respectively. Changing the direction of the magnets' shift allows generation of left or right helicity. The EPU produces the maximum power (K= 10.4, 2.4 kW) at the minimum gap of 14.0 mm and provides the widest operational energy range in the horizontal polarization mode. Horizontal polarization is considered the default operation mode for experiments.

The beamline design follows the concept of the collimated plane grating monochromator. A side-cooled toroidal mirror (M1) is the first optical element in the beamline, mounted 12.00 m from the centre of the undulator. It collimates the beam in both directions: horizontally and vertically. After M1, two pairs (vertical and horizontal) of precise baffles (BAFF) are used to limit the monochromator's aperture (acceptance angle). The monochromator was manufactured by FMB Feinwerk und Messtechnik GmbH, Berlin. It contains an internally cooled plane mirror (M2) and three slots for side-

cooled plane gratings. Currently, two Au-coated plane gratings are installed (PG1 with 600 l/mm and PG2 with 92 l/mm). The selected grating disperses incoming radiation in the vertical plane and - with the adjusted position and incidence angle of the M2 mirror - guides the central energy of the outgoing radiation in the direction parallel to the incoming beam. The branch line used in the experiments is selected by inserting either of the two toroidal focusing mirrors, $M3_{GP}$ or $M3_{SS}$, into the beam path. That mirror focuses the dispersed radiation at the exit slit, which is located 6.00 m downstream from the focusing mirror. After the exit slit, each branch line contains a higher-order suppression unit (HOS), where two optical filters (fused silica, MgF_2) and four thin film metal filters (In, Sn, Mg, Al) are mounted on two linear manipulators; i.e., each manipulator has a holder for three filters. These sets of filters allow the suppression of higher order radiation at photon energies below 72 eV. An ellipsoidal mirror ($M4_{GP}$ or $M4_{SS}$) refocuses monochromatized radiation at the end station in each branch. It deflects the beam sideways, keeping it in the horizontal plane. The entrance and exit arms of the refocusing mirror have been chosen to be 15% longer in the gas-phase branch than in the solid-state branch, so that the end stations are physically not mounted exactly side by side.
The summary of optics characteristics is presented in Table 2.1.

Table 2.1. *Parameters of the optical elements. Slope errors are given in the form tangential slope error/sagittal slope error.*

Optical element	M1	M2	PG1	PG2	$M3_{GP}$	$M3_{SS}$	Exit slit	$M4_{GP}$	$M4_{SS}$
Shape	Toroid	Plane[a]	Plane[a]	Plane[a]	Toroid	Toroid	Rect-angle	Ellip-soidal	Ellip-soidal
Deflection	Hor	Vert	Vert	Vert	Hor	Hor	–	Hor.	Hor.
Distance, mm	12,000	Var.			15,000	15,000	21,000	28,475	27,500
Incidence angle	88°	90°–70°			88°	88°	–	88°	88°
Opt. size, mm	500×20	490×20	140x25	140x25	400×40	400×40	0…4×0…2	414×46	360×40
Substrate material	Si	Si	Si	Si	Si	Si	–	Zerodur	Zerodur
Coating; thickness, Å	Au 866	Au 400 Pt 80	Au 320	Au 310	Au 679	Au 636	–	Au 400	Au 400
Roughness, Å	2.8	1.1	1.7-3.3 1 (blaze facet)	<2 79±15 (blaze facet)	1.6	2.0	–	1.7	2.0
Slope error, arcsec	0.21/0.68	0.066/0.037	0.039	0.043	0.12/0.44	0.11/0.47	–	0.68/2.46	0.37/0.48
Entrance arm, mm	12,000	–	–	–	∞	∞	–	7475	6500
Exit arm, mm	∞	–	–	–	6000	6000	–	2875	2500
Parameters									
R	691.1 m	123.5 km	72 km	61 km	343.9 m	344.4 m		–	–
r		31.9 km	>20 km	>20 km				–	–
ρ, mm	836.2	-	–	–	420.2	420.2		–	–
a, mm								5175	4500
b, mm								161.8	140.7
y0, mm								144.9	126.0
z0, mm								−2301	−2001
φ								0.889°	0.889°
Groove density			600 l/mm	92 l/mm				–	–
Blaze Angle			1.90°	4.2°				–	–

2.1.2. Beamline performance and comparison with the design values

Energy range

The beamline was designed to cover the photon energy range from 4.3 to 1000 eV when delivering horizontally polarized radiation. Other polarization modes were estimated to have higher minimum energies: 6 eV for circular polarization, 7 eV for vertical polarization and 11 eV for 45° inclined polarization. It was suggested that the highest photon flux at high photon energies would be achieved by utilizing the undulator in a wiggler mode, i.e., having the minimum undulator gap (14 mm) and largest possible beamline acceptance.

In practice, minimum energies produced by the EPU have been found to be 4.5 eV for horizontal polarization and 6.4 eV for vertical polarization. Minimum energies for inclined and circular polarizations are effectively limited by preservation of polarization by optics, which is described below in more detail.

An attempt to use the wiggler mode revealed an issue: overheating of M1. The issue is described in detail in section 2.2.1. Instead, high undulator harmonics (21-43) have been used to cover the high photon energy range. It has been possible to obtain useful photon flux up to 1300 eV.

Photon flux

The photon flux that can be exploited in an experiment depends on the exit slit width (which determines photon energy resolution), the monochromator's input acceptance, selected photon energy, selected undulator harmonic, and the amount of detuning of the photon energy from the central cone energy of the used undulator harmonic. The combination of these parameters also determines other important properties of the photon beam. For instance, the use of the central cone energy and relatively small acceptance allows one to reach a small focal spot size in the experiments and to reduce the contribution of even undulator harmonics. On other hand, one can achieve higher photon flux by setting the photon energy below the central cone energy and by opening the monochromator's acceptance.

In general, it is a complicated task to optimize the beamline parameters in order to obtain desirable beam properties among photon energy resolution, photon flux, size and shape of the beam spot, and presence of even harmonics, especially taking into account that different applications have rather diverse requirements for the photon beam.

As a reference, we present photon flux curves measured with the acceptances of 215x260 μrad (hor x vert) in the photon energy range 4.5-400 eV and 90x135 μrad in the photon energy range 400-1300 eV (Fig. 2.2) when the storage ring was operating with 400 mA electron beam current.

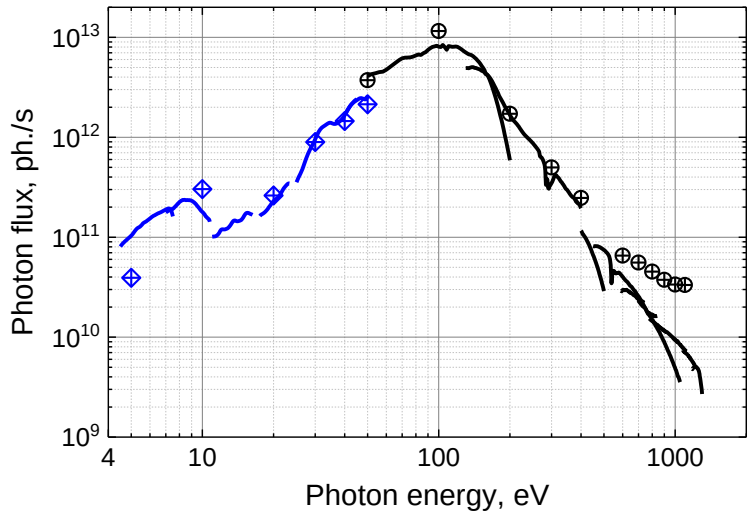

Figure 2.2. *Photon flux at the end station with 400 mA ring current and a fixed 20 μm exit slit width. The black curve represents photon flux obtained with the 600 l/mm grating. The blue curve represents photon flux obtained with the 92 l/mm grating and using an appropriate filter. Circles and diamonds show photon flux calculated in the same conditions for the 600 and 92 l/mm gratings, respectively.*

Current response from an Opto Diode AXUV-100 photodiode installed in the GPES was used to obtain the value of photon flux. This response was corrected for the diode's quantum efficiency taken from the manufacturer's datasheet. In the photon energy range 4.5 – 50 eV, different filters were used in order to decrease the impact of higher diffraction orders. In Fig. 2.2, black and blue curves represent

the measured photon fluxes obtained with the 600 l/mm and 92 l/mm gratings, respectively, using a fixed monochromator exit slit width of 20 μm. These data are compared to the simulated results (dots and diamonds). The undulator flux was estimated using SPECTRA v10.2 software for the harmonics described earlier. The raytracing model in the RAY-UI software was utilized to estimate the transmission of the photon entering the acceptance aperture in the sample plane. For the points in the energy range 4.5-50 eV, flux was also corrected for the transmittance of the filters.
As can be seen in Fig. 2.2, the experimental and the calculated photon fluxes are in good agreement except for a noticeable discrepancy at the photon energies above 500 eV. The differences between experiment and the simulations can be attributed to contamination of the mirrors and the gratings. A clear indication of the carbon and oxygen contamination can be seen in the measured photon flux at around 280 and 530 eV, respectively.

Polarizations

In contrast to horizontal and vertical polarizations, production of circular or inclined polarization under an arbitrary angle require the determination of the values of magnets' shift at every photon energy with the help of a polarimeter. The undulator's parameters were optimized in the range 20 - 200 eV for two cases: circular polarization (both left and right) and inclined polarization with a so-called magic angle (54.7°) between the horizontal direction and the electric field vector. As the phase shift induced by the beamline cannot be reversed in the inclined and helical modes of undulator, the resulting polarization state will be, strictly speaking, always elliptical. We can characterize quality of the polarization state by its linear polarization degree *PL*. Figure 2.3 shows energy dependence of the linear polarization degree measured (dots) and calculated (lines) for circular (black) and inclined (blue) polarizations. Circles and solid lines represent measurements and calculations for the 600 l/mm grating, respectively, whereas diamonds and dashed lines represent measurements and calculations for the 92 l/mm grating, respectively. Qualitatively, the experimental behavior of *PL* is in good agreement with the calculations, even though the calculations seem to underestimate phase delay introduced by the beamline optics. Using the 600 l/mm grating, polarization quality remains quite good down to 50 eV. At lower photon energies, the incident angles on M2 and grating become steep, which introduces a large phase delay. The 92 l/mm grating is operated at much shallower incident angles than the 600 l/mm grating. Its use preserves an acceptable quality of the polarization at low photon energies, but at the cost of lower photon energy resolution.

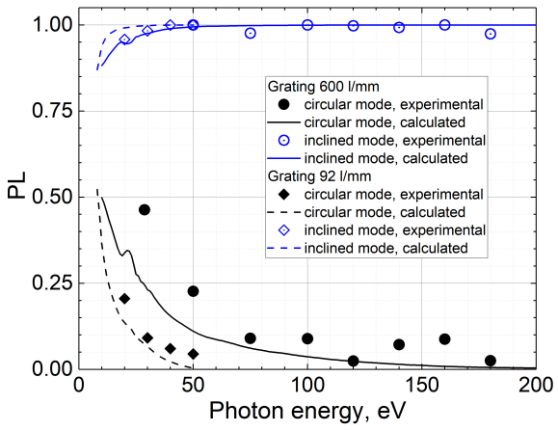

Figure 2.3. *Linear polarization degree PL for circular polarization (black solid points) and inclined polarization (blue open points) measured with the 600 l/mm (dots) and 92 l/mm (diamonds) gratings. Solid and dashed lines with corresponding color show calculated dependences of PL for the 600 and 92 l/mm gratings, respectively.*

The EPU of FinEstBeAMS is planned to be upgraded to operate in a so-called Universal mode, which will allow the phase shift of the undulator radiation to be adjusted as well (see section 8.1). After its implementation, we expect to provide pure circular and inclined polarization of radiation in the full energy range.

Photon energy resolution

The primary operation mode of the monochromator uses the fixed-focus constant c_{ff} = 2.25, which provides a good compromise between high order suppression, photon energy resolution and photon flux. The monochromator performance presented below was obtained with c_{ff} = 2.25 unless otherwise mentioned. The control system, however, allows the operation of the monochromator with different c_{ff} values, thus giving a possibility to increase photon resolution or photon flux, if required by a user.

The photon energy resolution of the beamline was investigated by measuring the total ion yield (TIY) spectra of several gases at the GPES. For that purpose, the Ne 1s → 3p, Ne 2p → 13d, N_2 N 1s → π*, Ar $2p_{3/2}$ → 4s, and Xe $5p_{1/2}$ → 9s resonances were used. Some selected spectra are displayed in Fig. 2.4.

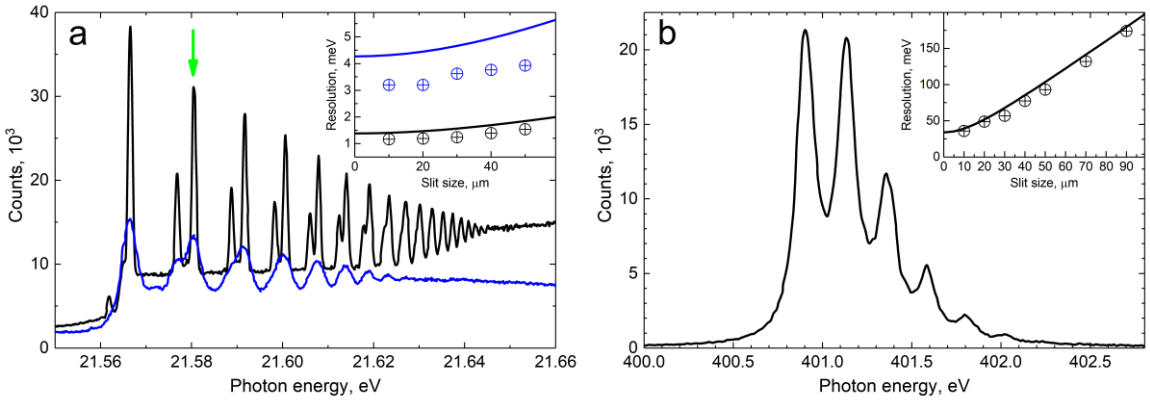

Figure 2.4. *Total ion yield spectra measured at (a) Ne 2p → nd,ms and (b) N_2 N 1s → π* excitations using the 600 l/mm grating (black line) and 92 l/mm grating (blue line). In the inset: experimentally obtained (dots) and calculated (solid line) dependencies of resolution on the slit width for corresponding graphs.*

The experimental core-excitation spectra were fitted with the Voigt profiles, where the Lorentzian widths in the final fits were fixed to the following values based on the data in the literature: 111 meV for the Ar $2p_{3/2}$ → 4s excitation, 112 meV for the N 1s → π* excitations in N_2, and 256 meV for the Ne 1s → 3p excitation. The Ne 2p and Xe 5p excitation spectra were approximated by the Gaussian functions, as the contribution of lifetime widths in these spectra were assumed to be negligible. The experimental photon energy resolutions, obtained with a 10 μm slit, and the corresponding resolving powers are presented in Table 2.2. Dependences of the photon energy resolution as a function of the monochromator exit slit width were measured as well. They are shown with dots for the corresponding spectra in the insets of Fig. 2.4.

Table 2.2. *Photon energy resolution and corresponding resolving power values obtained using a 10 μm exit slit width.*

		92 l/mm grating		600 l/mm grating	
Transition	Energy, eV	Resolution, meV	Resolving power	Resolution, meV	Resolving power
Xe $5p_{1/2}$→9s	12.89	2.58	5000		
Ne $2p_{1/2}$→13d	21.59	3.20	6700	1.17	18400
Ar $2p_{3/2}$→4s	244.39			28	8600
N_2 N1s→π*	401.10			36	11000
Ne 1s→3p	867.12			140	6200

Theoretically, the photon energy resolution of the beamline was estimated by taking into account four main factors: source size, exit slit width, slope errors of the optical elements and the diffraction limit. The calculated resolution agrees well with the experimental values except for the cases where the diffraction limit of the grating (at low energy range) or the exit slit width gives a dominant term to the photon energy resolution. In these cases, the calculations tend to overestimate the resolution, i.e., underestimate the resolving power. In the case of the exit slit contribution, this overestimation was taken into account by introducing a multiplier of 0.8 into the exit slit term. Examples of comparison between the calculated (solid line) and experimentally obtained resolution (symbols) are presented in the insets of Fig. 2.4.

In this way, we could estimate the photon energy resolution in a wide energy range and with different values of slit widths (Fig. 2.5). The calculated values are expected to reproduce well the experimental resolution apart from a slight overestimation in the low-energy range. In Fig. 2.5, dash-dotted lines are shown as eye-guides for some values of constant resolving power.

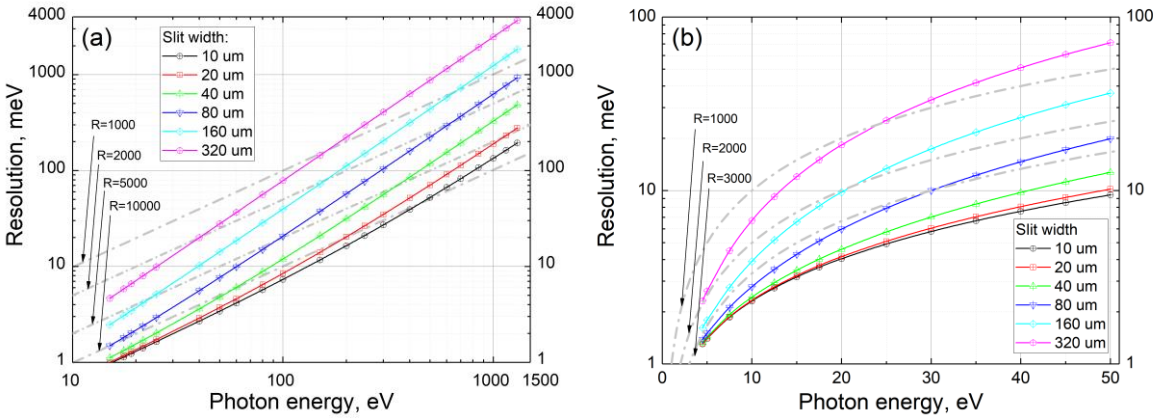

Figure 2.5. *Calculated photon energy resolution for (a) 600 l/mm grating and (b) 92 l/mm grating. Corresponding values of slit width are shown in the plot legend.*

The design goal for the beamline was to provide resolving power in the range 5000-10000 with the 600 l/mm grating. That goal has been achieved.

Focal beam spot size

Gas-phase electron spectroscopy and photoluminescence techniques do not have strict requirements for a beam spot size; they can be satisfied with the beam spot of a couple of hundred micrometers without significant losses in performance. In contrast, electron spectroscopy of surfaces and interfaces, conducted at the SSES, could benefit from a smaller beam spot. However, a high beam divergence in the low energy range and space constraints in the experimental hall resulted in the choice of a relatively small demagnification factor of 2.6 for the M4 mirrors at both branches and modest spot sizes at the end stations. With an expected horizontal spot size of 220-320 μm at the monochromator exit slit, the focal beam spot size should be of the order of 100x100 μm^2 in the major part of the operation range for a horizontally unrestricted beam and monochromator exit slit sizes of several hundred of micrometers. A pair of horizontal baffles have been installed before the monochromator exit slit. It allows us to decrease the horizontal size of the beam spot if needed in some applications.

The beam spot size was visualized using an yttrium aluminium oxide garnet crystal doped with cerium (YAG:Ce) and installed on a sample holder in the analysis chamber of the SSES. The crystal had a metal

grid on the surface with 1 mm step and 200 μm ticks for size reference, and the image of the beamspot was captured using a long-focus microscope equipped with a camera.

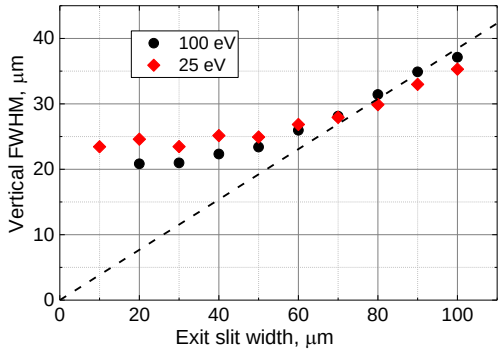

Figure 2.6. *The dependence of the vertical beam spot size on the monochromator exit slit width measured at the photon energies of 25 eV (diamonds) and 100 eV (dots). An "ideal" dependence (an exit slit width divided by the demagnification factor) is shown by a dashed line.*

Figure 2.6 presents the dependence of the vertical beam spot size on the monochromator exit slit width at photon energies of 25 and 100 eV. As can be seen, the vertical beam spot size deviates from the ideal dependence for slit widths below 80 μm and approaches a constant value of 20-25 μm. The horizontal beam spot size of the unrestricted beam practically showed no dependence on photon energy and remained in the range of 80-100 μm for photon energies above 10 eV. With the use of the horizontal baffles at the exit slit, it was possible to limit the horizontal beam spot size down to about 30 μm.

2.2. Shortcomings and solutions

2.2.1. Overheating of the first mirror

The first mirror (M1) receives most of the heat load among the beamline's optical elements. It cannot currently dissipate the heat produced by the photon beam in some conditions. In particular, the beamline cannot be used in the wiggler mode. Instead, high undulator harmonics with relatively open gaps are used in the high energy region, leading to a 2-3 times lower photon flux than what could have been achieved in the wiggler mode. The smallest undulator gaps are only used to reach the lowest photon energies.

The overheating of the M1 mirror will also become a problem when the electron beam current in the storage ring is increased from 400 mA to 500 mA; the latter value is the design goal. In recent tests with 500 mA, overheating was observed with undulator gaps below 20 mm (using optimal acceptance for the first harmonic). A possible future use of this higher ring current would force us to decrease acceptance, resulting in loss of the photon flux.

At some of other beamlines, heating of the M1 mirror has been concluded to arise from an electrode that collects photocurrent from the mirror. To overcome this issue, the Veritas beamline has disconnected the electrode from the mirror and it has received a separate holder with integrated water cooling. At FinEstBeAMS, we plan first to calculate if changes made by Veritas could help solve overheating of M1 at FinEstBeAMS. If the calculations are promising, the same design will be utilized. Otherwise, additional changes will be needed.

2.2.2. Leak in the monochromator's cooling circuit

After the installation of the 92 l/mm grating in 2018, a vacuum leak appeared in the gratings' cooling circuit during the baking of the monochromator. As replacement parts were not available for the leaking cooling circuit, we decided to pump both the cooling line and its guard vacuum line to mitigate the problem. Heat load on the gratings is relatively small and can be sustained even without cooling. The monochromator chamber was opened again in 2019. One section of the cooling line was replaced

in 2019. However, two other leaking spots caused by corrosion in a guard vacuum pipe and a flange. were discovered in the cooling line. A replacement of the whole cooling section has been delivered to FinEstBeAMS, but it has not been installed.
Some other beamlines at the facility have experienced corrosion in the cooling lines of the M2 mirrors. As FinEstBeAMS uses an M2 mirror from the same supplier (In-Sync), concerns have been raised about possible corrosion happening in the M2 cooling lines. The situation is complicated by the fact that neither cause nor solution to this corrosion problem is known. Early indications of extensive corrosion are monitored (ions levels in the water, presence of water in guard vacuum), while work is ongoing at the facility to understand and address the issue.

2.2.3. Higher orders of diffraction and scattered light

Since our first measurements in the low photon energy range, we noticed presence of radiation originating from higher diffraction orders of grating. By analysing the photoelectron spectra of a gold foil, we found that the peaks arising from the diffraction orders 2-9 have the same total intensity as the peak arising from the first diffraction order. Estimations made utilizing a photodiode, which is sensitive to all high energy radiation, show that the overall intensity of the high energy radiation is 2-5 times greater than intensity of the first harmonic. Even though not all the properties of this high-energy radiation are completely understood, it was concluded that its most probable cause is light scattered on the diffraction grating.
To mitigate the issue, the installation of an additional Al-coated grating in the monochromator has been proposed. The design was developed internally: the grating should have the best performance in the energy region 10-13 eV, which is the most problematic region not covered by a filter. The profile of the grooves is optimized for suppressing the 3rd order of diffraction (a comparison of calculated efficiencies of different diffraction orders between the existing and designed gratings is shown in Fig. 2.9a). Higher line density of 360 l/mm will result in steeper grating angles, which, in combination with Al coating, leads to much lower reflection efficiency for radiation with energy above 70 eV (Fig. 2.9b).

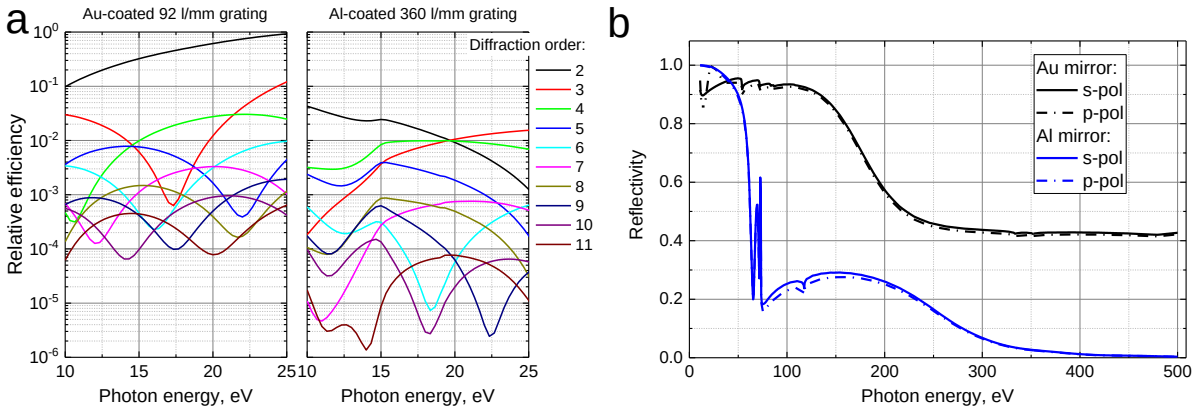

Figure 2.7. *(a) The efficiency of higher diffraction orders normalized to that of the first diffraction order, calculated for the existing 92 l/mm Au-coated grating (left) and the proposed 360 l/mm Al-coated grating (right). (b) Comparison between reflectivity dependences of Al and Au mirrors on photon energy for the mirrors' angles corresponding to the 13 eV position of the gratings with c_{ff}=2.25.*

This project is done in collaboration with University of Tartu (Estonia), which have secured funding for procurement of the grating. It was found that no company on the market can directly manufacture the grating in time required by the funding terms. It was decided that the acquisition of the grating will be done in two stages: first, the grating blank will be acquired from Zeiss, and second, ruling and coating

of the blanks will be done later at BESSY. The procurement documents for the grating blanks are now under preparation.

2.2.4. The accessibility of photon energy ranges

The FinEstBeAMS EPU is the strongest undulator at the MAX IV facility with K= 10.4 at the minimum gap of 14 mm. It strongly affects the electron orbit in the ring, resulting in orbit stability problems and inability to top-up electrons when the EPU gap is close to its minimum value. The issue was partly solved after the installation of additional correction magnets in summer of 2021. We can now operate the gap freely in horizontal polarization, but the accelerator cannot still top-up the current when the undulator has a small gap in vertical polarization and in some other phases. The problem is complicated by the interaction of the FinEstBeAMS EPU with other undulators, mainly with that of Bloch, which is the second strongest undulator.

2.2.5. Carbon contamination

Carbon contamination was visible on the surfaces of the M1 and M2 mirrors since the beginning of the beamline operation. The absorption band of C 1s (around 280 eV) was observed in the photon flux curve (Fig. 2.10, black curve). This contamination was especially severe in the monochromator as it has been vented two times due to the leak in the cooling line.

An oxygen leaking system was mounted in the optics hutch in November 2020 to perform so-called "oxygen cleaning". The oxygen was dosed into the monochromator and M1 vacuum chambers to create pressure in the range of 10^{-8}–10^{-7} mbar. The cleaning has been performed in several steps, gradually increasing oxygen pressure and monitoring changes in photon flux.

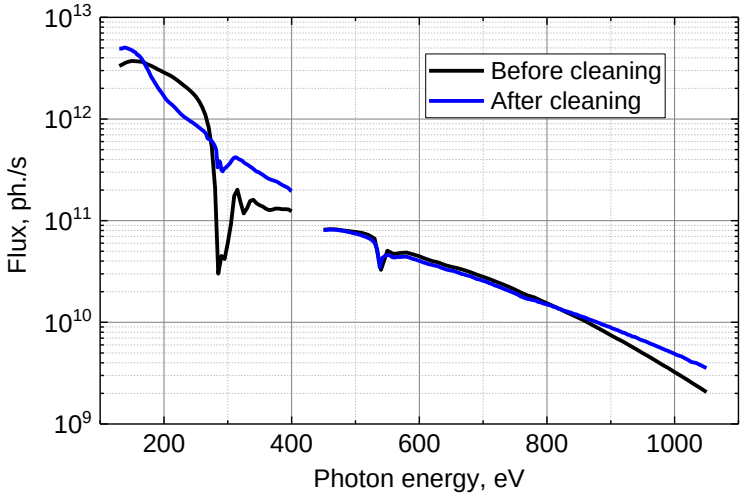

Figure 2.8. *Photon flux before (black curve) and after (blue curve) oxygen cleaning.*

As a result, intensity of C 1s absorption has been reduced (Fig. 2.10, blue curve) and oxygen leaking has been stopped. It was also observed that oxygen cleaning increased the photon flux in the range from 130 to 160 eV, but decreased it in the range from 160 to 270 eV. We have found no explanation for these two changes in the photon flux. The latest measurements done in September 2022 show that carbon contamination has become worse without O_2 dosing, hence we will likely start the cleaning procedure again, but with a slightly lower pressure of O_2 in the monochromator chamber (low 10^{-8} mbar range).

3. Gas-phase end station

3.1. Technical description

K. Kooser *et al* [3.1] have published an instrumental paper about the gas-phase end station (GPES). That article concentrates on the experimental setup used for photoelectron-photoion coincidence (PEPICO) spectroscopy. The main equipment of the GPES comprise a Scienta R4000 electron spectrometer and an ion time-of-flight spectrometer, which is capable of 3D ion momentum imaging and multi-ion coincident detection. We summarize the main features of the GPES in this review report; the reader is referred to the original publication for more details. In addition, FinEstBeAMS offers to the users two other experimental setups for coincidence experiments, namely, a negative-ion/positive-ion coincidence (NIPICO) setup and a magnetic bottle electron spectrometer (MBES). They are also described below.

3.1.1. Vacuum system

The vacuum chambers and the support of the GPES are shown in Figure 3.1. The main vacuum chamber is basically an asymmetric six-way cross with two DN200CF flanges in one direction - along the photon beam - and four DN160CF flanges at every 90 degrees in the perpendicular direction. The electron spectrometer is mounted on a DN160CF flange and the ion TOF spectrometer is usually mounted opposite to the electron spectrometer, but it can also be removed if it is not needed in an experiment. The remaining two DN160CF ports of the six-way cross chamber can be used for, e.g., a sample delivery system, an additional detector, or a cold trap. However, the full openings of the ports are not available because the GPES vacuum chamber has μ-metal shields along all inner walls to block out external magnetic fields. The DN200CF flanges are closed with custom-made reinforced reducer nipples with DN40CF end flanges. The vacuum chamber is supported on these nipples via three metal wheels on each side. By connecting the nipples to a rotary seal and a flexible bellow, the whole vacuum system can be rotated around the main axis of the six-way cross, which coincides with the direction of the photon beam.

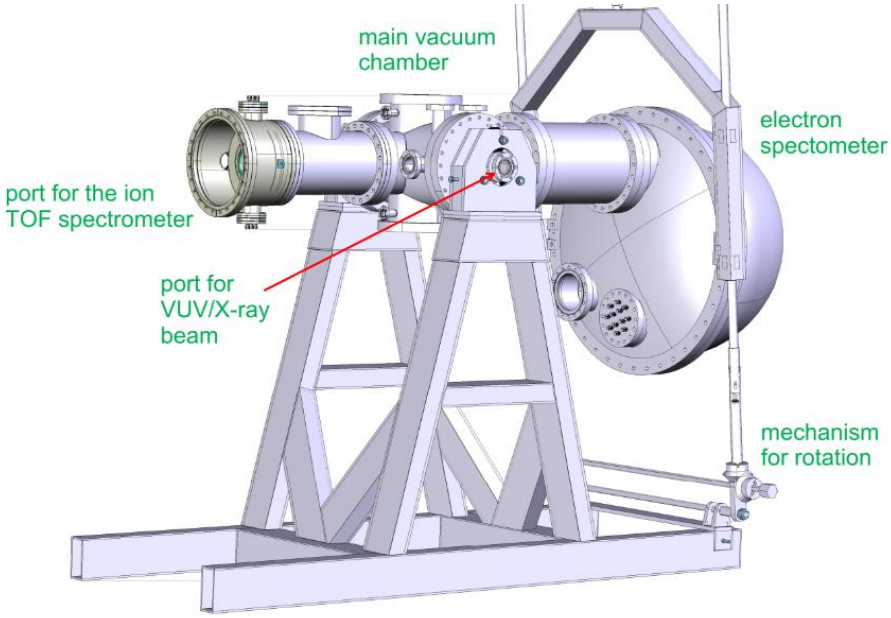

Figure 3.1. *A drawing of the GPES shows the Scienta R4000 electron spectrometer positioned in the horizontal direction (0°). An ion TOF spectrometer is mounted opposite to the electron spectrometer. Only its vacuum chamber is shown here. The vacuum chambers can be rotated around the photon beam so that the electron analyser moves to a vertical position (90°).*

The hemisphere of the electron spectrometer and the vacuum chamber of the ion TOF spectrometer have DN100CF ports where two 300 l/s Pfeiffer HiPace 300 turbomolecular pumps are installed for pumping. A 14-cm long capillary, welded to a double-sided DN40CF flange, and an 80 l/s turbo-molecular pump are mounted in a vacuum section between the GPES main chamber and the end of the beamline. The vacuum system helps decrease the pressure from $1 \cdot 10^{-5}$ mbar, which can be used in the GPES main chamber during experiments, to 10^{-8} mbar range at the downstream end of the differential pumping section, which is a permanent part of branch A, and further to the 10^{-10} mbar range in the last mirror chamber (M4).
The stand of the GPES rests on a large, almost square frame (160 cm x 200 cm) made of hollow stainless steel bar with 10 cm x 10 cm cross section. The support mechanisms below the frame allow a fine adjustment of the chamber's position with respect to the photon beam. This frame – and the stand and the vacuum chambers on it – can be moved by several tens of cm along the photon beam on linear rails that are fixed on the floor. A translation of about 60 cm is needed when another experimental setup is mounted on the movable frame after the GPES main chamber and brought to the focal point of the beamline. In such events, the 80 l/s turbomolecular pump and a beam pipe containing the 14-cm capillary are removed from the vacuum system. The ion TOF spectrometer is also removed because an entrance hole for the photon beam in its nozzle (see Fig. 2 in Ref. [3.1]) could cut part of incoming radiation. This removal reduces the pumping capacity of the vacuum chamber because the 300 l/s turbomolecular pump attached to the ion TOF spectrometer also goes away. It can be compensated for by mounting a 700 l/s turbomolecular pump directly on the GPES main chamber.

3.1.2. Electron-ion coincidence setup

The GPES has been designed for coincidence measurements between photoelectrons (or Auger electrons) and photoions resulting from the same photoionization process. The Scienta R4000 electron spectrometer has a hemispherical analyser with a mean radius of 200 mm. For the purpose of coincidence measurements, its original detector has been replaced by a fast resistive anode position-sensitive detector. The time-of-flight (TOF) ion spectrometer has a RoentDek detector equipped with 80-mm microchannel plates (MCP) and Hex-anode delay-line setup.
A simplified working principle of the electron-ion coincidence setup is shown in Figure 3.2. Some components are not included in the figure; for instance, the electron lens of the Scienta R4000 spectrometer is missing. In a PEPICO experiment, the electron spectrometer is set to measure electrons within a fixed kinetic energy window, the width of which depends on the chosen pass energy. When an electron is detected, a fast signal is passed from the electron detector to data acquisition electronics, which leads to a quick ramp-up of voltages in the repeller and extractor electrodes around the interaction region and a generation of a START signal for a TOF measurement. The resulting electric field accelerates ions from the interaction region toward the ion TOF spectrometer. If ions are detected within a predetermined time window of the START signal, their hit positions on the hex-anode delay line detector (six coordinates for one ion) and flight times are registered. The electron hit's X position from a Quantar position analyser is added to the information of the coincidence event collected by the RoentDek's data acquisition program (CoboldPC). After a calibration, the X position can be correlated with the kinetic energy of the detected electron.
The energy analysis of the ejected electrons enables the determination of the initial electronic state of the created photoions. The data from the TOF spectrometer allow users to retrieve the final state momentum of the ion in all three spatial dimensions.
Not all users want to perform PEPICO experiments. The Scienta R4000 electron spectrometer can be used for high-resolution electron spectroscopy. Kinetic energy resolution depends on the combination

of the selected pass energy and the entrance slit before the hemispherical analyser. As usually, there is a trade-off between resolution and count rate, so the measurement of an electron spectrum with the highest possible resolution is generally not feasible due to insufficient count rates. On the other hand, too high count rates can lead to saturation of the detector, which affects the shapes and intensities of the peaks in the spectrum. The saturation count rate is about $1.5 \cdot 10^5$ Hz.

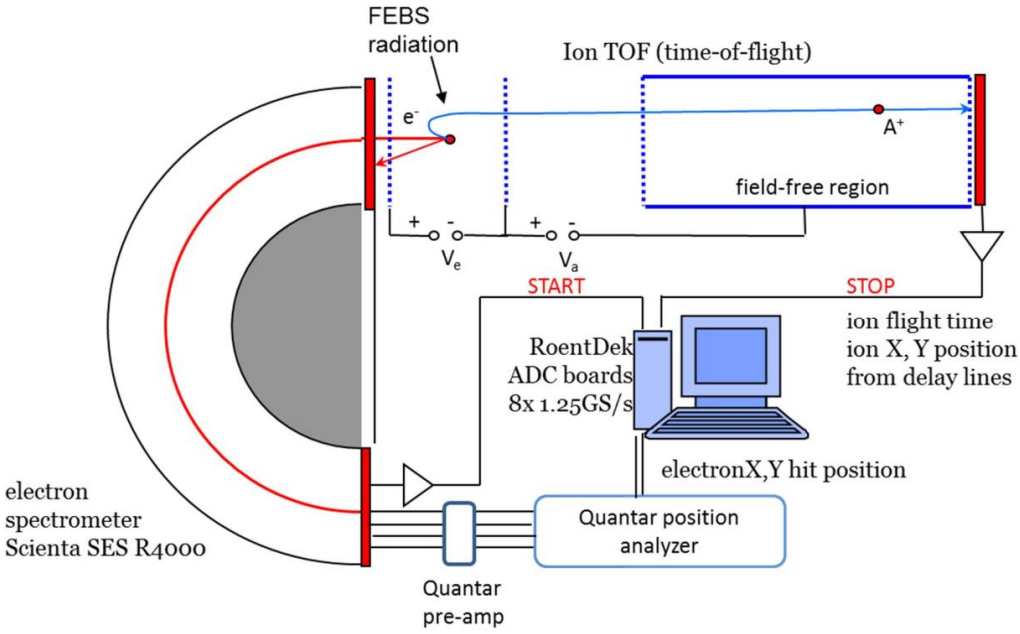

Figure 3.2. *The main components and working principle of the electron-ion coincidence setup. An electron detected with the Scienta R4000 electron spectrometer is used to ramp up an extraction field in the interaction region and to give a START signal for a time-of-flight measurements of ions. The arrivals of the ions in the detector of the TOF spectrometer give STOP signals for the TOF measurement. The hit positions of electrons and ions on the detectors are also registered.*

The ion TOF spectrometer can be used independently to study fragmentation of sample molecules. In that case, a pulse generator is configured to give START signals for ion TOF measurements, typically at the frequency of 10 kHz, and to ramp up the electric field in the interaction region. The electric field is kept up longer than what is the flight time of the heaviest ion of interest. As the photon energy range of FinEstBeAMS begins from 4.5 eV, ion TOF spectrometry can be practised to determine the first ionization energies of almost all molecules as well as to determine appearance energies for ionic fragments. When the measurement of ion TOF spectra is coupled with the scanning of the incident photon energy and the undulator gap, one can extract partial ion yields. This measurement mode is not well developed because the RoentDek computer and the beamline control computer do not talk with each other. We have asked a software specialist from KITS Software to look at this problem.

After the publication of Kooser *et al.*'s article [3.1], the Scienta analyser's control program was migrated from a Windows XP computer to a Win-10 based computer in June 2021 because the use of an obsolete control computer was considered a safety risk. At the same time, the hardware for controlling the voltage supplies was partly upgraded: an SES Digital Output Motherboard was installed in the new control PC and an inlet plate was mounted on the back of the high-voltage rack of the Scienta voltage supplies to allow Ethernet communication between the PC and the rack. A National Instruments counter card in the Win-10 computer was also upgraded. The data acquisition program was modified by KITS-Software in order to function in the Win-10 environment. The new control system was used in three beamtimes at the GPES in September and October 2021. Unfortunately, it

crashed several times. The frequency of the error depended on count rates: scans could be completed with low count rates, but not with high ones. Our contact person from KITS-Software found that the problem was caused by the new counter card. After the addition of some error handling, the Scienta analyser's upgraded control program has been stable at all kinds of counts rates.
The GPES can be coupled with external sources for experiment of less common samples. Three biggest sources are described here briefly. First, a liquid-jet source from FlexPES has been mounted at the GPES for electron spectroscopy studies of atmospherically relevant samples. Two spacer flanges were needed to compensate for slightly different dimensions of the vacuum chambers at the FlexPES and FinEstBeAMS, but no other changes were required for the use of the liquid-jet source. Second, a cluster source ("MUSCLE") from the University of Oulu has also been used at FinEstBeAMS. A dedicated support with versatile adjustment mechanisms was constructed for it. A large Pfeiffer A204H fore-vacuum pump with 160 m^3/h pumping capacity was acquired to work as a backing pump for the cluster source's two 2000 l/s turbo pumps. It could be used for other purposes at FinEstBeAMS or other MAX IV beamlines, but this has not happened yet. Thirdly, an aerosol delivery system has been developed in collaboration between the LDM team at MAX IV and an aerosol research group at the Division of Ergonomics and Aerosol Technology of LTH, Faculty of Engineering. See section 7.4 for more details of the aerosol delivery system.

3.1.3. Negative-ion/positive-ion coincidence setup

FinEstBeAMS can offer users an experimental setup for the detection of coincidences between negative and positive ions. It consists of two ion TOF spectrometers. The one for positive ions is borrowed from the PEPICO setup described above. A TOF spectrometer for negative ions was designed and constructed at MAX IV, but it was used initially for a couple of years at the Gas-phase Photoemission Beamline at Elettra, Trieste (Italy) [3.3]. It has been brought back to MAX IV and it now belongs to FinEstBeAMS. The two ion TOF spectrometers were first mounted in the replica chamber of the GPES and commissioned in March 2020. Later Christian Stråhlman (Malmö University) received a grant for the construction of a dedicated end station for negative-ion/positive-ion coincidence (NIPICO) spectroscopy. This development project only involved acquisition of a vacuum system, vacuum equipment and some electronic components.

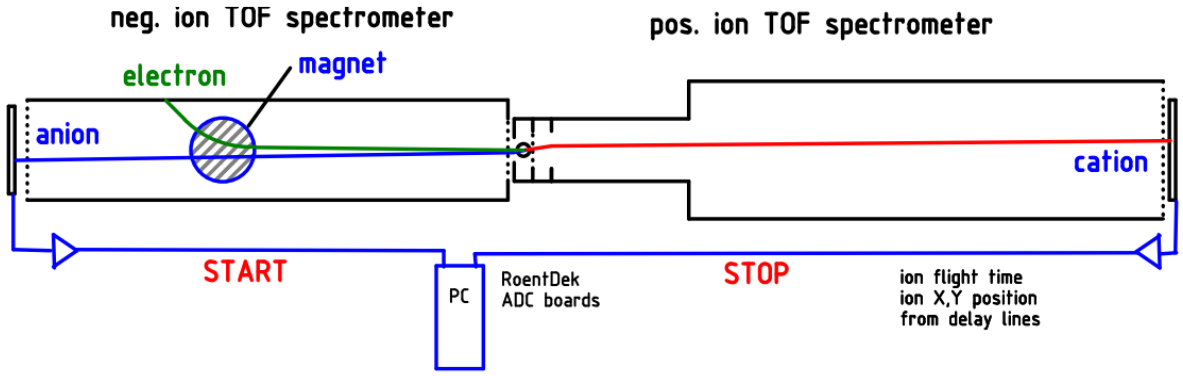

Figure 3.3. *Scheme of the NIPICO setup. Negative and positive ions created in the interaction region (the circle at the centre of the drawing) are accelerated by constant electric fields towards the MCP detectors. Most electrons that would disturb anion detection are deflected with a magnetic field.*

The NIPICO instrument is schematically shown in Figure 3.3. It uses the same CoboldPC program for data acquisition as the PEPICO setup of the previous subsection. The X-position signal from the Scienta analyser to the RoentDek computer has been replaced with a signal from the MCP detector of the

negative ion TOF spectrometer. The CoboldPC program could be used directly in NIPICO experiments; only some parameters in the configuration files had to be changed. We perform NIPICO experiments using a constant extraction field in the interaction region. Signals from the negative particle detector function as START signals and those from the positive particle detector as STOP signals. We do not measure directly the flight times of negative and positive ions, but rather their differences (arrival time differences, ATD). The CoboldPC program can also register events where positive ions arrive before negative ions. The multi-hit capability of the positive ion detector allows the observation of events where several positive ions are emitted together with one negative ion.

3.1.4. Magnetic bottle electron spectrometer

(The text in this section is courtesy of Andreas Hans.)

A magnetic bottle electron spectrometer (MBES) has been set up and commissioned by the Nano and Molecular Systems Research Unit (NANOMO) from Oulu, Finland for permanent availability at FinEstBeAMS. In the first commissioning experiments with single-bunch operation of the 1.5 GeV ring in February 2020, a team of collaborators from Oulu and Kassel, Germany, measured the first time-of-flight electron spectra. It was demonstrated that despite the relatively short circulation period of 320 ns (= maximum temporal distance between two consecutive exciting pulses), electron spectra from one individual bunch could be extracted by making use of coincidences. The main purpose of the installation of the magnetic bottle spectrometer is the investigation of UV- and X-ray induced dynamics in clusters, nanoparticles, and aerosols. In a second beamtime, the MBES was therefore combined with a source for prototypical rare gas clusters.

The working principle of a MBES is such that a strong permanent magnet (~1 T) close to the intersection point of sample and synchrotron radiation acts as a magnetic mirror and turns all electron trajectories into one direction. Opposite to the permanent magnet, a drift tube is mounted. Weaker magnetic fields (~1 mT) produced by solenoids prevent electrons from getting lost before they reach the microchannel plate detector at the end of the drift tube. It is possible to apply accelerating or decelerating fields in order to adjust the time of flight. A section view of the drift tube (about 2.2 m long) is shown in Fig. 3.4.

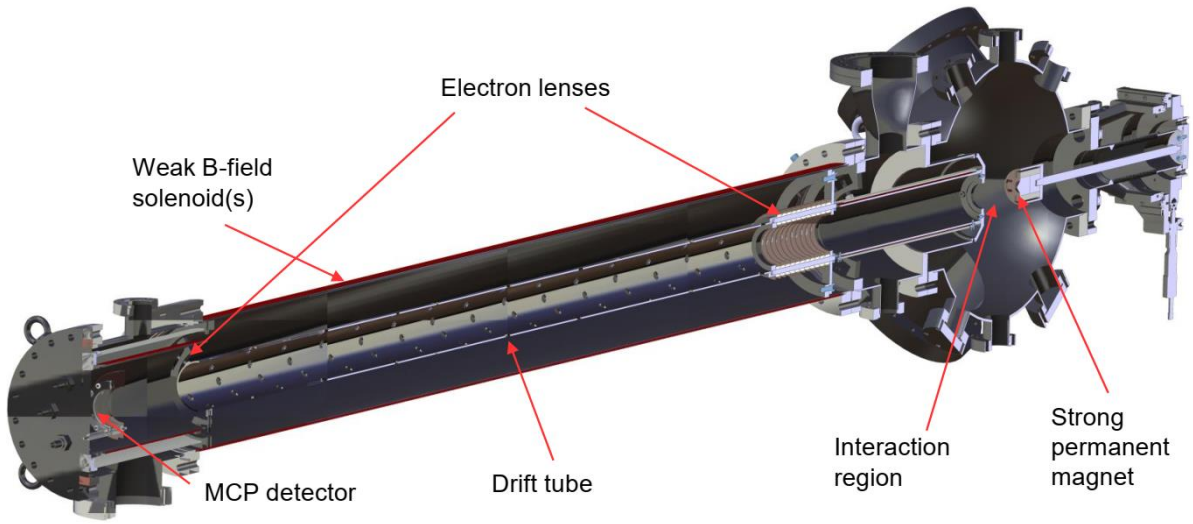

Figure 3.4. *A section drawing of the magnetic bottle electron spectrometer that is available for users at FinEstBeAMS. A different vacuum chamber has been used for the MBES at FinEstBeAMS. The spectrometer can provide useful data only in single-bunch mode.*

3.1.5. Comparison with other gas-phase beamlines

FinEstBeAMS has been designed as a multipurpose beamline. Therefore, it is not straightforward to compare the performance of the FinEstBeAMS with that of dedicated gas-phase beamlines. Among the existing gas-phase beamlines, the characteristics of FinEstBeAMS resemble most those of the PLÉIADES beamline at Soleil synchrotron in France. A new gas-phase beamline ("MOST") has been designed for the future upgrade of the Elettra storage ring in Trieste. It has not been funded yet, but it is interesting to know what kind of properties are considered important for a future gas-phase beamline. The main parameters of the FinEstBeAMS, PLÉIADES, and MOST are given in Table 3.1. The photon energy resolution of FinEstBeAMS is slightly worse than that of PLÉIADES and MOST. On the other hand, FinEstBeAMS offers access to lower photon energies than the other two beamlines and very competitive photon flux in part of the photon energy range.

Table 3.1. *Comparison of characteristics of three gas-phase beamlines.*

	GPES at FinEstBeAMS	PLÉIADES [3.3]	MOST [3.4] (Design)
Location	MAX IV, Sweden	SOLEIL, France	Elettra 2.0, Italy
Years of operation	2019-	2008 (?) -	After 2026 if funded
Light source	Apple II type undulator with 95.2 mm period	1) 5-m long electromagnetic undulator, 256 mm period; 10-100 eV 2) 2-m long Apple II type undulator, 80 mm period; 35-1000 eV	1) Low energy undulator, fixed gap, variable phase; 8-200 eV with the first harmonic 2) High energy undulator (EPU), 50.6 mm period; 80-3000 eV with harmonics 1, 3, and 5
Monochromator	cPGM	PGM using varied line spacing (VLS) and varied groove depth technologies	At intermediate and high photon energies like the BOREAS beamline [3.5] (3 spherical premirrors + 3 VLS plane gratings)
Photon energy range	G2: 4.5 – 50 eV G1: 15 – 800 (1300) eV	10 – 1000 eV (four gratings)	10-3000 eV
Polarization	Linear H, V In progress: inclined, circular (11-200 eV)	10 – 40 eV: linear H, V 35 – 1000 eV: linear H, V, tilted, elliptical	1) Linear H (20 eV -), V (8 eV-), circular (14 eV -) 2) Linear H (84 eV -), V (143 eV -), circular (112 eV -)
Resolving power (R)	5000 (12.89 eV with G2) 18400 (21.59 eV with G1) 11000 (400 eV)	15000 (10-40 eV) 20000-100000 (35-1000 eV)	25000 at 100 eV (600 l/mm), 14500 at 400 eV (1200 l/mm), 9000 at 1500 eV (1800 l/mm)
Photon flux	1×10^{14} photons/s/0.1% BW at 100 eV 2×10^{12} photons/s/0.1% BW at 400 eV	1×10^{13} photons/s/0.1% BW at 100 eV	($1\text{-}2\times10^{15}$ photons/s/0.1% BW at source)
Spot size on sample	100×100 μm^2	50(H) × 30(V) μm^2 (Branch 2) 180(H) × 100(V) μm^2 (Branch 3)	25(H) × 20(V) μm^2 at 100 eV (using 2 KB mirrors)
Experimental setups	PEPICO, NIPICO, MBES	High-resolution electron spectrometer, electron-ion coincidence setup with PSDs	

3.2. User operation

Until now the weekly working cycle at MAX IV Laboratory has been such that Mondays have been reserved for accelerator studies and Tuesdays for beamline commissioning. Beamtimes have been scheduled from Wednesday 08:00 to Monday 08:00, which comprises 30 shifts. That has been the standard length of the general users' beamtimes at FinEstBeAMS. Now that the SSES has begun user operation, beamtimes of different lengths could be scheduled more easily also at the GPES (and the PLES). In the spring 2023 semester, most Tuesdays will be given to normal beam delivery.

Gas-phase users typically arrive one or two days before the beginning of their beamtimes, depending on how much preparation work is needed for their experiments at the beamline. If an exchange of the experimental setup between the GPES and the PLES is needed, the FinEstBeAMS staff perform that work in the previous week, if allowed by the beamtime calendar, or on Monday and Tuesday in the week of the actual beamtime. The latter option is acceptable only if the GPES does not require complicated installations for the users' experiments that can take 1-2 days of working time. The FinEstBeAMS staff can make these changes ready for the users or, at the very least, participate in the installation work together with the users. Examples of the biggest installations comprise those of the cluster source, which is owned by the University of Oulu, and the aerosol delivery system, which has recently been developed at MAX IV (see section 7.4). The installation of the magnetic bottle electron spectrometer is also a major operation. It is actually not used with the main GPES vacuum chamber, but it is mounted in the so-called user (or replica) chamber downstream of the GPES main chamber. The latter is moved closer to the beamline, which requires the removal of the beampipe and the HiPace 80 turbopump from the GPES. When the NIPICO setup is used for experiments, it is mounted in the same position as the MBES. In some cases, the users install their equipment in the GPES by themselves because only they know what to do, while the FinEstBeAMS staff can offer help in coordinating work with MAX IV resource groups such as plumbers for making gas-line connections or the vacuum group for performing a leak check.

Most gas-phase users have performed experiments previously at FinEstBeAMS and they know the beamline and the GPES rather or even very well. Therefore, formal training is usually not given to such recurring users before the beamtime. A paper copy of the user instructions of the GPES is available to the users at the beamline (and as a file at Google Drive). A brief introduction to the beamline control system can be given to new members of the experimental teams. The quality of the training could be improved. On the other hand, it is often difficult to define when gas-phase experiments really begin, if the users and staff already work together with the installation of the equipment before the formal beginning of the beamtime. Additionally, the users can often begin their experiments on Tuesday evening, if the photon beam becomes available and when the beamline staff members have already gone home.

3.3. Shortcomings and development

Integration of the end-station data acquisition software into the MAX IV control system

Problem: A major problem at the GPES is that the software controlling the measurements is not integrated into the MAX IV control and data acquisition system. In other words, the end station and beamline computers are not talking to each other. For example, there is no straightforward way to start automatically the measurements of electron or ion TOF spectra, while scanning the photon energy or any other parameter.

Partial solution: The Scienta spectrometer of FinEstBeAMS is included in a MAX IV project for the integration of the Scienta and SPECS electron spectrometers into the MAX IV control and data acquisition system. For Scienta spectrometers, this integration will be implemented using the PEAK platform of ScientaOmicron. The Scienta R4000 spectrometer of FinEstBeAMS is compatible with PEAK after the recent hardware upgrade. Despite the modified detector of our spectrometer, the planned development should be possible at least for the measurements of conventional electron spectra.

Without solution: The (RoentDek) computer controlling the measurements of the ion TOF spectra and electron-ion coincidence spectra should also be integrated into the MAX IV control and data acquisition system. This is probably a question of resources, as such integration has been done for the RoentDek detector of the ICE end station.

Gas handling system

Problem: FinEstBeAMS still does not have a permanent gas handling system. Its construction was started in 2018, when gas lines were drawn from three fire-safe gas cabinets toward the end station. The work was interrupted because some vacuum equipment could not be selected due to lacking safety regulations at MAX IV. It was later found with X-Ray radiography that some welds in the installed gas lines were badly made. They were repaired in autumn 2020.

Temporary solution: Since 2019 FinEstBeAMS has used a temporary ventilated gas cabinet for the experiments of flammable, oxidizing and toxic gases.

Final solution: The Central Project Office coordinates the construction of gas handling systems at different beamlines. We have been told that the installation of the gas system at FinEstBeAMS will continue in autumn 2022. If that happens the gas handling system should become ready in 2023.

Obstacles in the development of instrumentation

Problem: Presently, the beamline scientist who is responsible for the GPES acts as a beamline manager. He cannot devote sufficient time to the technical development or characterization of the end station's instrumentation. Consequently, the development of the GPES instrumentation has been neglected. Looking beyond the manpower problem, fewer proposals are and will likely be scheduled at the GPES after user operation began properly at the SSES. Lack of beamtime is becoming a threat for successful LDM research at FinEstBeAMS.

Short-term solution: FinEstBeAMS would need a technically oriented staff member whose responsibilities should include the development and maintenance of the GPES instrumentation.

Long-term solution: The construction of a dedicated LDM beamline would give LDM researchers much more possibilities to develop their instrumentation and research at the whole MAX IV Laboratory.

Exchange of the end stations

Problem: The experiments at Branch A require frequent exchanges of the end stations. This is not an ideal situation. If the GPES is aligned very carefully for some (coincidence) experiments, the alignment will be lost when the chamber is moved out of focus for other experiments. When the GPES is brought back to the focus point, the vacuum chamber's position will be slightly different. Mounting and dismounting the end stations increases the risks of accidents for both persons and equipment. The beamline staff use plenty of time and energy for this kind work. The resources could be used better for other purposes.

Possible solution: There is no good short-term solution in sight. We already try to minimize the number of the exchanges of the setups through scheduling of the beamtimes. A long-term solution would be the construction of a dedicated LDM beamline, allowing the installation of more permanent end stations.

REFERENCES

[3.1] K. Kooser et al., "Gas phase end-station of electron, ion and coincidence spectroscopies for diluted samples at the FinEstBeAMS beamline of the MAX IV 1.5-GeV storage ring", J. Synchrotron Rad. **27** (2020) 1080.

[3.2] C. Stråhlman et al., "A tandem time-of-flight spectrometer for negative-ion/positive-ion coincidence measurements with soft x-ray excitation", Rev. Sci. Instrum. **87** (2016) 013109.

[3.3] https://www.synchrotron-soleil.fr/en/beamlines/pleiades

[3.4] R. Totani et al., "MOST beamline @ Elettra 2.0 – optical layout", (unpublished technical report, private communication by K.C. Prince).

[3.5] A. Barla et al., "Design and performance of BOREAS, the beamline for resonant X-ray absorption and scattering experiments at the ALBA synchrotron light source", J. Synchrotron Rad. **23** (2016) 1507.

4. Photoluminescence end station

4.1. Technical description

The main goal of the photoluminescence end station (PLES) is to enable luminescence spectroscopy under vacuum ultraviolet (VUV) and soft X-ray excitations. Any materials in solid phase (single crystals, glasses, ceramics, films, powders, etc.) can be studied.

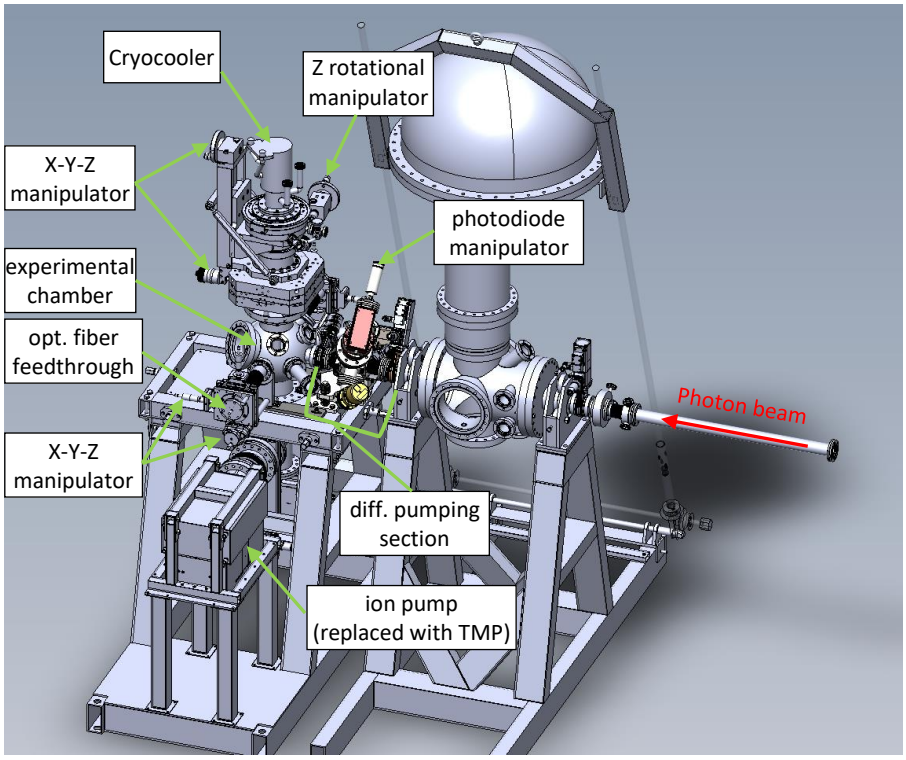

Figure 4.1. *A drawing of the PLES connected to the GPES with description of its main parts.*

The PLES was designed to be a removable end station that can be connected downstream of the GPES (Fig. 4.1). The main experimental chamber of the luminescence setup has a spherical shape with a diameter of 26 cm. It is pumped by two Pfeiffer HiPace 300 turbo pumps mounted on a 4-way cross that is connected to the bottom of the main experimental chamber. The initial version of the PLES utilized one turbo pump and one ion pump, but, after initial stage of operation, the ion pump was replaced with a second turbo pump. The main chamber of the PLES is connected to the GPES end station through an additional differential pumping section, which has two 10 mm apertures and Pfeiffer Vacuum HiPace 80 turbo pump, in order to protect the main UHV chamber from potential residual gas contamination from the gas phase experiment. The differential pumping section also accommodates a manipulator with two AXUV-100G photodiodes. These photodiodes can be moved into the beam path and are used for recording excitation photon flux.
The end station is equipped with a closed-cycle helium cryostat with a cold-finger type sample holder. The cryostat consists of an ARS DE-204PB cryocooler and an ARS-4HW compressor (from Advanced Research Systems). The size of the two-sided sample holder is large enough (20x90 mm^2) to accommodate dozens of samples on each side. It has an integrated heater, and, using a LakeShore 335 temperature controller, it is possible to regulate temperature of the samples from 6 to 320 K. The cryocooler, mounted on a rotational stage, is installed on an XYZ manipulator, facilitating the alignment of the samples with respect to the incident beam.

Two optical fibers are used to collect photoluminescence signal. One of them is optimized for the UV-VIS range, the other one for the VIS-NIR range. The fibers (together with vacuum feedthroughs) are mounted on two XYZ manipulators, which are fixed on the opposite ports of the vacuum chamber in the horizontal direction (perpendicular to the beam).
The experimental chamber has numerous ports that are suitable for mounting equipment in various geometries for other kinds of measurements (or to be used as viewports for alignment). A port located at an angle of 45° to the beam direction can be used for reflection measurements, whereas a port on the downstream side of the chamber can be used for absorption measurements.
Luminescence detection is performed by an Andor Shamrock SR-303i-B spectrograph equipped with a set of 300 l/mm gratings (blaze wavelengths 300, 500, 1200 nm) on a rotational turret. The spectrograph can be connected to the end station by one of two optical fibers, matching the spectral range of the fibers mounted in the experimental chamber. A mirror condenser is used to focus light from the optical fiber on the input slit of the spectrograph. The Andor Shamrock spectrograph has two exit ports: one of them is permanently occupied by a Newton DU9 70P-BVF CCD detector, whereas the other is equipped with a motorized exit slit to which an external detector can be mounted. The following detectors are available at the beamline: Hamamatsu H8259, H8259-01 and H8259-02 photon counting heads, a thermoelectrically cooled infrared NIR PMT Unit Hamamatsu H10330B-45, and a thermoelectrically cooled hybrid photodetector Becker & Hickl HPM-100-07C for time-resolved measurements. The detectors are working in photon counting mode and connected to a National Instruments NI6602 counter board.
The CCD is suitable for measurements in the spectral range 200-1100 nm. Spectra in a wavelength window of 270 nm can be measured in single acquisition by the CCD when using a grating with line density of 300 l/mm. The Hamamatsu photon counting heads of 8259 series cover the wavelength range from 200 to 850 nm and, since the integration of the CCD into the data acquisition system, they are mostly used only for an initial sample alignment. The NIR PMT Unit H10330B-45 is effective in the spectral range of 950-1350 nm. The hybrid photodetector HPM-100-07C for time-resolved measurements can be used in the wavelength range 220-850 nm.
Luminescence measurements are mostly done in steady-state mode, as the operation parameters of the storage ring (700 ps bunch length with 10 ns interval) are not suitable for time-resolved measurements. Time-resolved measurements can be performed when the ring operates in single-bunch mode: time interval between the electrons bunches is 320 ns in this case, whereas the bunch length is compressed down to about 180 ps. The time-resolved measurements are implemented using the method of time-correlated photon counting: a start marker is taken directly from the ring clock, photons are detected by the HPM-100-07C detector and registration of the events is carried out by a Cronologic xTDC4 time-to-digital converter card. The beamline control system allows one to measure both time-resolved emission and excitation spectra. The FWHM of the instrument response function of the system is about 180 ps and it is limited by the length of the electron bunch.

4.1.1. Comparison of photoluminescence beamlines

A short comparison between the experimental capabilities of the PLES and other photoluminescence beamlines is presented in table 4.1. The data for the SUPERLUMI and HOTRLU beamlines were taken from several available sources [4.1–4.5] and should be approached with caution: numbers in these sources do not exactly agree with each other. It should also be noted that parameters like flux and resolving power usually have complex dependence on the photon energy and substituting them with a single number is only usable for a rough comparison.

Table 4.1. *Comparison of characteristics of photoluminescence beamlines.*

	FinEstBeAMS PLES	SUPERLUMI	BL3B (HOTRLU)
Location	MAX IV, Sweden	DESY, Germany	UVSOR-III, Japan
Years of operation	2019-	1981-2012, 2021-	2013-
Light source	Undulator	Bending magnet	Bending magnet
Excitation energy range	4.5 – 50 eV 15 – 1300 eV	3.7 – 40 eV	1.7-31 eV
Maximum resolving power (R)	3000 (4.5 eV)–5000 (50 eV)	16000 (3.7 eV) – 1500 (40 eV)	2000 (6.8 eV) – 5000 (>10 eV)
Photon flux	2×10^{12} with R=2000	2×10^{11} with R=600	1×10^{10} with R=1000
Spot size on sample	100×100 μm^2	200×5000 μm^2	750×250 μm^2
Luminescence detection spectral range	200-1100 nm 950-1350 nm (UV- VIS monochromator)	110-600 nm (VUV-Pouey monochromator) 200-1200 nm (UV- VIS monochromator)	UV-VIS monochromator, PMT, CCD detectors. Precise wavelength ranges are not specified.

4.2. Operation

The end station operation is split in weekly cycles due to necessity of venting the vacuum chamber for the installation of samples. To avoid loss of actual beam time, the samples installation is usually carried out on an accelerator maintenance day (Monday). The samples are glued on the surface of the cryostat's sample holder using thermally conductive silver-based glue. Samples in form of a powder have to be pressed into copper pallets. After the installation, the baking with duration of 12-14 hours is required to facilitate pumping. Arrival of users, sample installation and baking take in total about 36 hours. A user beamtime usually starts on Wednesday morning, as Tuesdays are reserved for beamline development. If no actual beamline commissioning is scheduled on Tuesday and the photon beam is available, the users could start their measurements already that day. During the application submission, users can request single-bunch operation to conduct time-resolved measurements. If the single-bunch operation is granted, it is scheduled on Tuesday and typically lasts for 23 hours.

Training is required before users can carry out measurements independently: the software solutions used for the beamline control system, namely Tango with Taurus GUI and Sardana framework, are specific for the accelerator facilities and rarely used outside by photoluminescence community. Taking also into account general complexity of the beamline control system, new users need 2-3 days to become familiar with the experimental setup. A typical photoluminescence experiment consists of a big number of relatively short measurements. That requires the presence of at least one well-trained operator and creates a constant workload on him. For that reason, users usually work in 2-3 shifts, and the optimal size of the group has been found to be 4-5 people. The data acquisition system based on Sardana has an advantage in this regard, as it supports macros, which allow users to program sequences of measurements and to change parameters of the setup, automatizing the execution of similar measurements and decreasing the load on the operator.

Another important part of training is alignment of the samples and light collecting optics. Traditionally, samples alignment for the beam spot is done using white light coming from zero-order of monochromator. Luminescence emission is then collected by lenses or mirror. In our case, high photon flux provided by the undulator allows us to see luminescence emission of most samples with a bare eye, and adjusting an optical fiber is much simpler procedure than focusing an optical system with lenses. That generally simplifies and speeds up the sample alignment but it also requires some training, especially if luminescence is weak or if there is no emission in the visible range.

Photon flux for correction of excitation spectra has to be measured utilizing a photodiode with known quantum efficiency (AXUV-100G). Sodium salicylate, which is typically used for recording photon flux under VUV excitation, was found to be unstable under high photon flux; it degrades dramatically during the measurement time. Initially, photon flux curves were re-measured every week but week-to-week

differences were found to be negligible, therefore currently these measurements are done only during the first beam time in the experimental session.
Users also have to be trained on data processing, which is happening after they are able to do measurements. The Sardana saves the measurement data in the HDF files. The HDF is a convenient format for data storage on site, but limited number of data processing applications support it natively. Photoluminescence community mostly use Origin, which supports the HDF format very poorly. For convenient data transfer and processing, the python script converting data into ASCII format and set of import filters for the Origin were made.
Therefore, all trainings and measurements under supervision are done on the weekdays, and users continue their beam time alone through the weekend. On-call service is provided by staff for users in case any issues arise on the weekend.

4.3. Shortcomings and development

Design constraints

The main limitations of the end station originate from the design decision to make it removable. Nowadays, the PLES is installed at Branch A only for photoluminescence experiments. This results in the frequent installation and removal of the end station, which in turn puts strict limits on the weight, size, and possible complexity of the end station as well as on the duration of the installation procedure. As the installation of the PLES takes two days, it cannot be done in the same weeks as photo-luminescence experiments are scheduled.
Due to the design of the cryostat, the top flange has to be opened in order to extract the sample holder for the installation and removal of samples, i.e., the end station has to be vented. On the one hand, this allowed a very simple and cheap design of the cryostat and experimental chamber, on the other hand, it has greatly increased the time needed for sample installation as compared to load-lock systems. This design makes it much more convenient to install big batches of samples at the same time for measurements lasting the whole week of beamtime. If one liked to accommodate beamtimes that last less than a week, a huge dead time would be introduced due to the exchange of the samples. With the SSES coming online, this issue can be partly solved by filling this dead time with experiments at the other branch, but such scheduling is not always possible.
In a long perspective, any significant development of the PLES would require the end station to be placed at the beamline permanently or at least for much longer periods than is possible now. This would allow the design of a new PLES with a wider range of capabilities and optimized for user operation. Such a perspective is possible if a dedicated LDM beamline is constructed, allowing the GPES to be moved to the new beamline.

Higher order radiation

Photoluminescence measurements are affected by presence of higher order radiation and scattered radiation transmitted through the beamline's monochromator. The issue of higher order and scattered radiation is discussed in detail in section 2.2.3. To suppress these contributions, a set of optical (fused silica and MgF_2) and thin-film (In, Sn, Mg, Al) filters are used in the photon energy range 4.5-70 eV. There is a number of shortcomings arising from the use of filters. As each filter works in a limited energy range, full excitation spectra have to be constructed by sewing together several curves, which complicates data processing. Thin film filters have second transmittance windows in the range 100 - 1000 eV, so they do not remove completely artefacts originating from high energy radiation. No filter covers the energy range 10.7-12.5 eV. The proposed solution is to install an Al-coated grating, which would suppress both higher order of diffraction and scattered radiation (see section 2.2.3 for details).

Reflectance measurements

The PLES was initially planned to provide a possibility for collimated reflectance measurements using current response from a photodiode installed in the main chamber. The photodiode should be the same type as the one utilized for the photon flux measurements. It would provide stable response in a wide range of photon fluxes and energies and easy readout with an electrometer. However, we found that the current response of the photodiode is affected by luminescence of the sample. To solve this issue, the photodiode was moved away from the sample: the component of the luminescence signal should decrease as square root of distance, whereas the intensity of the reflected photon beam should not decrease much. But this led to another problem: as the size of the photodiode is relatively small (10x10 mm^2), it became practically impossible to adjust the sample to a correct position where the photon beam would be reflected on the diode.

Instead, we suggest to implement a detection technique that has been proved to work at SUPERLUMI: a viewport window covered with sodium salicylate from inside can be used as a wavelength convertor and its emission can be detected with a conventional PMT. The viewport window is relatively large (40 mm in diameter), sodium salicylate luminescence is not excited by visible light, and an UV band pass filter installed in front of the PMT cuts off possible luminescence from the sample.

Dead time in the measurements of excitation spectra

The measurements of excitation spectra require the movement of both the EPU gap and the monochromator energy, which typically takes about 6 s per step. High photon flux produced by the EPU allows one to use relatively short integration times (in range 1–4 s) for samples of average intensity, which are comparable with the movement time. Therefore, dead time related to the movement of the gap and the photon energy takes significant part of the total measuring time. The PLES would benefit from a continuous scanning project (see section 8.3), allowing one to eliminate the movement's dead time and increase throughput of the samples as a result.

Time-resolved techniques availability

Availability of the single-bunch delivery limits usage of time-resolved techniques at the PLES. In addition to very limited single-bunch weeks, single-bunch delivery only can be scheduled on some Tuesdays, in the very beginning of the user beam time, which is inconvenient for planning of the experiments. The accelerator team works on implementation of TRIBs (transverse resonance island buckets): in this mode, a single bunch of electrons will be located on a resonance orbit. The radiation from this bunch propagates in a different direction compared to the main beam. Re-aligning beamline optics to accept only this radiation would create “pseudo single-bunch operation mode”, while practically not affecting other beamlines. The first tests showed that radiation from TRIBs can be accepted by the beamline but a feedback system would have to be improved.

REFERENCES

[4.1] https://photon-science.desy.de/facilities/petra_iii/beamlines/p66_superlumi /unified_data_sheet/index_eng.html

[4.2] V. Pankratov, A. Kotlov. “Luminescence spectroscopy under synchrotron radiation: From SUPERLUMI to FINESTLUMI,” Nucl. Instrum. Methods Phys. Res. B. **474** (2020) 35-40.

[4.3] P. Gürtler et al. “Superlumi: A high flux VUV spectroscopic device for luminescence measurement,” Nucl. Instrum. Methods Phys. Res. B. **208** (1983) 835-839.

[4.4] https://www.uvsor.ims.ac.jp/beamlines/3B/ebl3b.html

[4.5] K. Fukui et al. “New VIS–VUV photoluminescence beamline at UVSOR-III,” J. Synchrotron Rad. **21** (2014) 452–455.

5. Solid-state end station

5.1. Technical description

5.1.1. Overview

The solid-state end station (SSES) has been designed as a high-throughput apparatus with flexible sample preparation options for X-ray photoemission (XPS), angle-resolved photoemission (ARPES), and X-ray absorption spectroscopy (XAS). The SSES is composed of four ultra-high vacuum (UHV) chambers connected by a distribution chamber*:* the analysis chamber, the preparation chamber, the storage chamber, and the load-lock chamber (see Fig. 5.1). The design of the system also allows sample transfer from a vacuum suitcase to the load lock and the preparation chamber. All the chambers can be pumped and vented independently. The main instrument is a SPECS PHOIBOS 150 R7 hemispherical electron analyser with a 2D delay line detector. The manipulator has 5-axis motorized motion: three linear motions and two rotational motions (polar and azimuth). An open cycle cryostat can be cooled either using liquid He or N_2. The preparation chamber is equipped with a low energy electron diffraction (LEED)/Auger setup and a quadrupole mass spectrometer. It is possible to quickly load, for example, an evaporation source or an evaporation cell without venting the main preparation chamber through a pumping manifold. In the following sections, each chamber will be described in detail. The SSES served its first external regular users in Jan 2022 for XPS and XAS experiments.

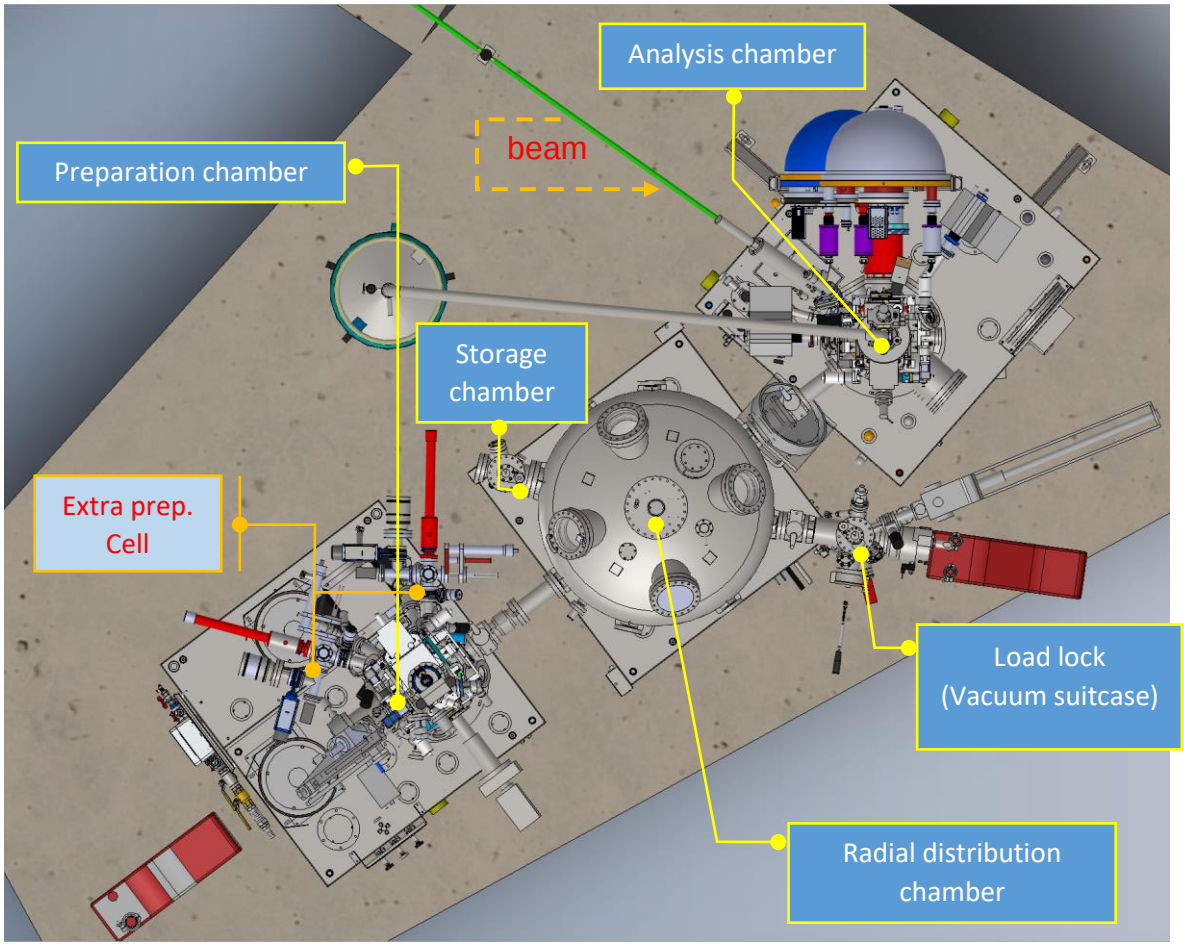

Figure 5.1. *Schematic representation of the SSES with the indication of the five individual UHV chambers and the photon beam. There are two possible mounting orientations of the electron analyser: its entrance slit can be either in the horizontal (grey) or vertical direction (dark blue in the image). Currently, the analyzer is mounted with the entrance slit in the vertical direction to facilitate angle-dependent studies utilising the manipulator's polar rotation.*

5.1.2. Radial distribution chamber

The radial distribution chamber (RDC) is used to move samples between different UHV chambers. Its transfer arm takes one sample at a time. Sample forward/backward translation and rotation of the arm (to align it with the different ports of the other chambers) are all coupled through a single rotational feedthrough, which is manually actuated. The procedure of a sample's attach/release from the transfer arm is illustrated in Fig. 5.2. Users can have up to 25 sample plates in UHV simultaneously, i.e., 12 in the load lock, 12 in the storage chamber (which has a sample carousel identical to that in the load lock) and one in the preparation chamber. The coordinates of the motorised manipulators in the analysis and preparation chambers corresponding to sample transfer positions have been saved in the manipulator software and only rarely need corrections (by beamline staff). The predefined measurement position is used as a starting point for fine adjustment depending on the sizes of the different samples.

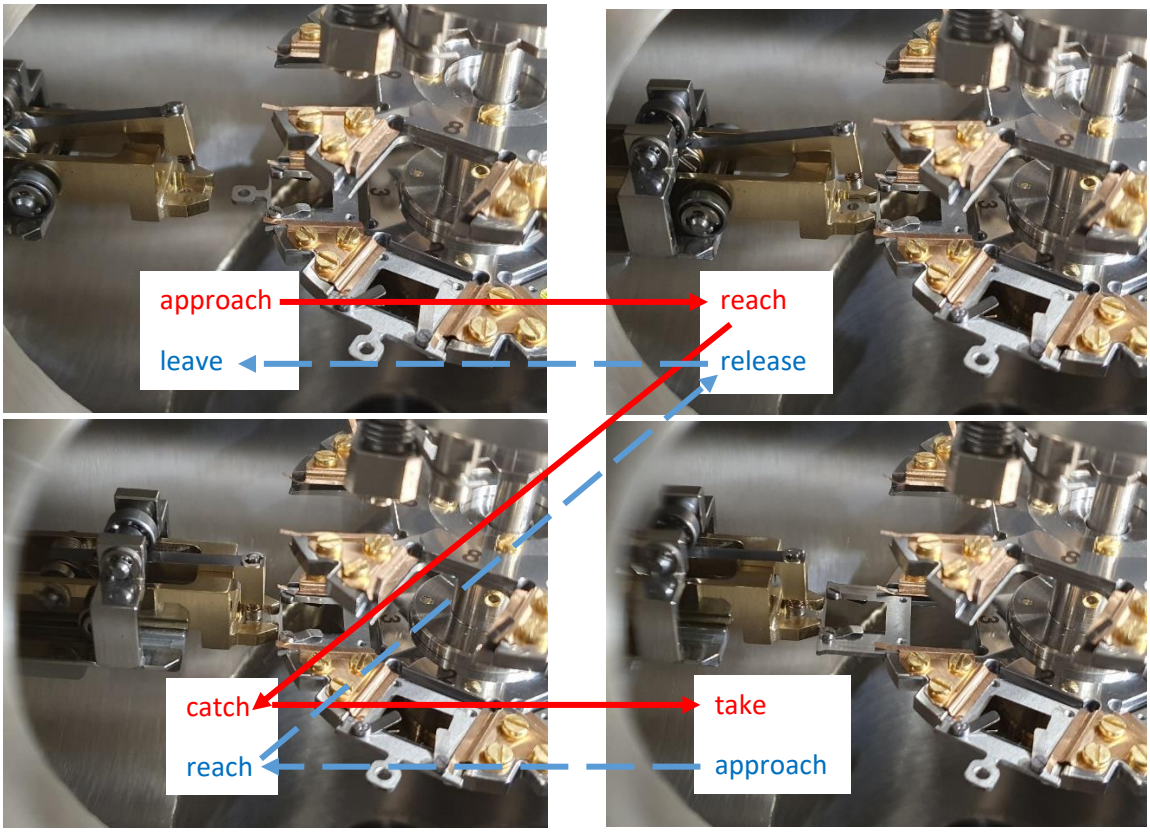

Figure 5.2. *Photographs of sample transfer in the Load Lock. The red and blue paths indicate taking and leaving the sample, respectively. All steps are done with a single manually rotatable knob: anti-clockwise rotation approaches the sample receiver; moving forward to the end; keep moving until a spring force to close the pin and catch the sample; Release the force slowly, making sure the pin is not open and take the sample from the receiver. Push forward one more time against the spring force, and the pin will open and leave the sample in the station.*

The end station is configured to accept Omicron-style flag sample holders, both flat plates for resistive and e-beam heating, and double-decker plates for direct-current heating (see Fig. 5.3).

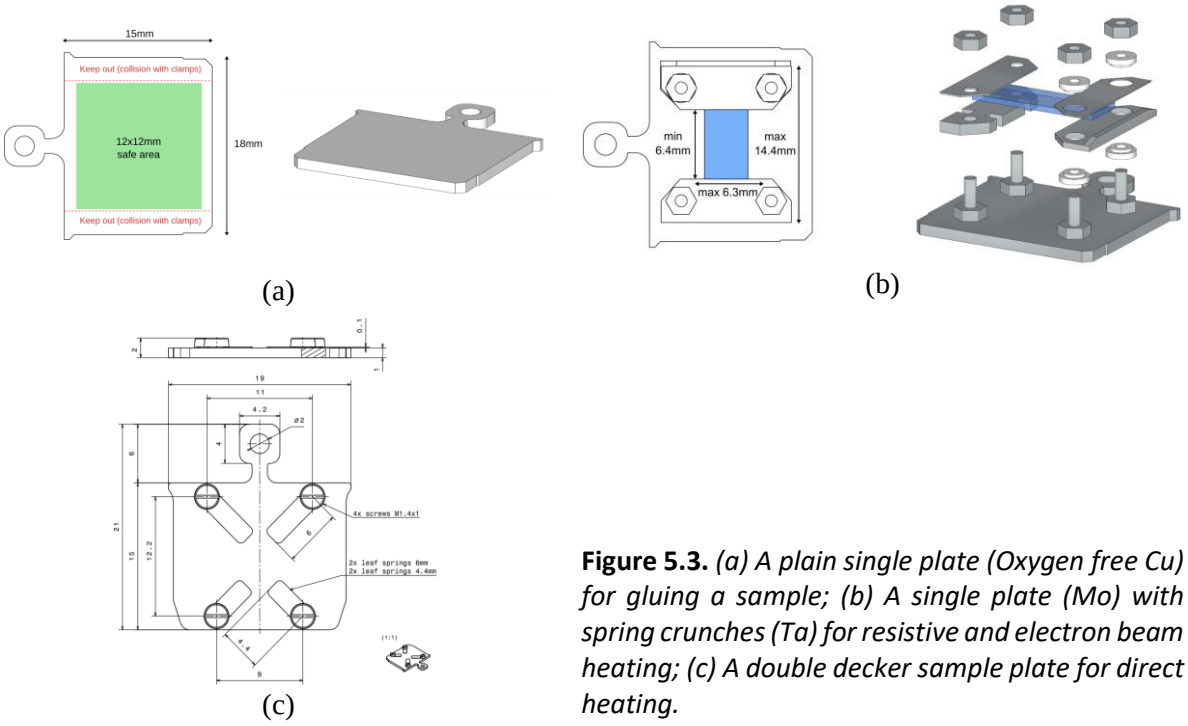

Figure 5.3. *(a) A plain single plate (Oxygen free Cu) for gluing a sample; (b) A single plate (Mo) with spring crunches (Ta) for resistive and electron beam heating; (c) A double decker sample plate for direct heating.*

Users are recommended to use sample holders provided by the beamline staff, which are tested to fit in any sample station in the SSES. However, users are also welcome to bring their own sample plates if the experiment is sensitive to contamination. We provide tantalum foil and wire for mounting single crystal samples and double-sided carbon tape for powder samples. A spot welder, a hot plate and spin coating are available in a chemical lab, which should be booked in advance.

5.1.3. Analysis chamber

The Analysis chamber is equipped with a SPECS PHOIBOS 150 R7 hemispherical electron analyser and a 40 mm 2D delay line detector (DLD) with less than 5 dark counts/s. The analyser has an integrated twofold µ-metal shielding and has energy resolution better than 2 meV at the lowest pass energies. Furthermore, the chamber is equipped with a Mg/Al dual anode (non-monochromatised) X-ray gun (PREVAC RS 40B1), which allows users to perform preparatory XPS measurements and commissioning offline. The chamber is made of μ-metal for magnetic shielding. In the bottom part of the chamber (near the measurement position), the residual magnetic field has been measured on site to be less than ~0.4 µT (~0.1% of the Earth's magnetic field).

Sample manipulations are accomplished using a 5-axis manipulator (Prevac 01-3025-3109-01031). The kinematic data of the motions are shown in Table 5.1. The range, precision and reproducibility of positioning is sufficient for most (even relatively demanding) experiments. The measurement geometry is shown in Fig. 5.4: the manipulator is mounted vertically with the polar rotation coupled through a differentially pumped rotational feedthrough and the azimuthal motion is driven directly by an in-vacuum motor. With the polar angle chosen at normal emission (NE), the X and Z translations are in the plane perpendicular to the electron lens'saxis, and the Y motion parallel to the axis. Furthermore, in order to align the beam spot to the lens's axis, the beam on the sample can be moved by the M4 mirror: the M4 pitch moves the beam spot along the X direction with the minimum step of 1 µrad (~8.5 µm at NE) and the M4 roll moves it in the Z direction with the smallest accessible step size of 1 µrad (~0.2 µm).

Table 5.1. *Kinematic data of the manipulator in the analysis chamber.*

Axis	Range of motion	Precision
X	±25 mm	1 µm
Y	±25 mm	1 µm
Z	50 mm	10 µm
R1 (polar)	±175 deg	0.1 deg
R2 (azimuth)	± 90 deg	0.1 deg

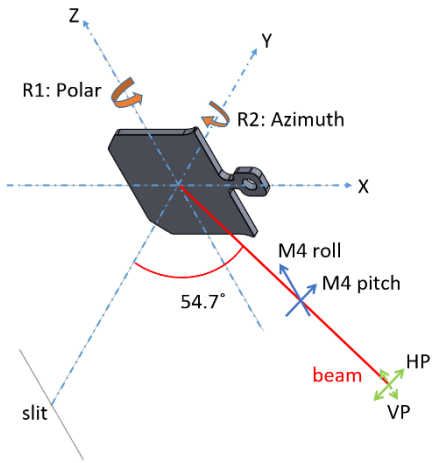

Figure 5.4. *Measurement geometry when the slit of the analyser is in the vertical direction. The observation detection (the electron analyser lens axis) is at 54.7˚ with respect to the photon beam's propagation direction. The actual normal emission angle depends on how the sample is mounted on the sample holder. Hence, a fine adjustment of the polar angle is needed for sensitive measurements (especially for ARPES); the direction of linear polarization of light is shown with green arrows. Solid blue arrows indicate the adjustable movement of the beam by the M4 mirror.*

The manipulator contains an integrated cryostat for LN_2 cooling. In the current setup, it takes about one hour to cool the sample (empty plate) down to 96 K and three hours to reach 92 K. Temperatures between this and RT can be freely chosen using the integrated counter-heater in the manipulator. The LN_2 dewar can be refilled without dismounting the setup, hence, in principle, cooling could last for a whole beamtime. Without such refills, one full dewar lasts at least 90 hours in a controlled flow. Liquid He cooling is also technically feasible, but this capability is still under commissioning. A sample could also be heated in the analysis chamber by resistive heating up to 500 K. However, it is not recommended in order to protect the detector of the analyser from outgassing of the sample and sample station. Temperature is measured by a K-type thermocouple connected at the lower clamp that is used to generate a good thermal contact by firmly holding the sample (Fig. 5.5). The clamp is required to be frictionally tight in order to prevent the sample from dropping during R2 rotation. Hence, the sample plates of the SSES have a very small tolerance (+50 ~-100 µm) of thickness, and similar for the width. Therefore, for user brought sample plates, there is a considerable risk that it could get stuck in the manipulator, or loose contact (temperature reading would not be reliable, R2 rotation would be risky).

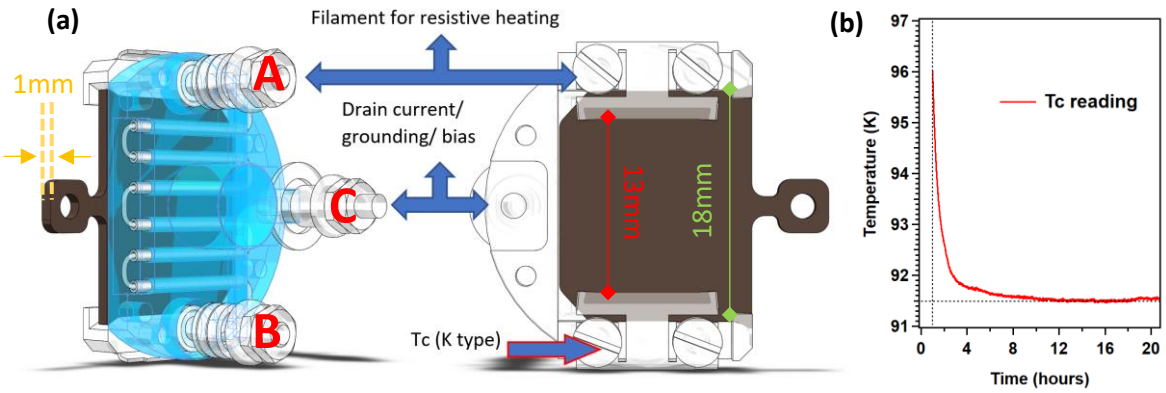

Figure 5.5. *(a) Drawing of one single plate in the sample station of the analysis chamber's manipulator. The electric connections A and B allow sending current to the filament for resistive heating. Connection C is used to ground/bias the sample for an XPS measurement and to measure drain current for an XAS measurement. A K type of thermocouple is connected to one of the screws for the measurement of the heating or cooling temperature. The transport piece (blue) is made of Mo, which connects to the cold finger of the cryostat. (b) Temperature curve measured from Tc connection shown in (a). Time scale was zeroed at the start of cooling when the pressure build-up valve on the dewar was fully open. Stable temperature at 91.5 K was achieved after 10 hours.*

5.1.4. Preparation chamber

The preparation chamber has been designed for sample treatment and growth. It is equipped with a 4-axis-two-sample-station manipulator (PREVAC), an ion source for sputtering (PREVAC IS 40C1), LEED/AES optics (OCI BDL800IR), thickness monitors (PREVAC TMC13), a quadrupole mass spectrometer (?) (QMS HAL 201-RC), three gas dosing lines, and free ports with valves for mounting sources without venting the chamber.

In the preparation chamber, we have different settings for cooling. A sample plate at a resistive heating station can be cooled down to ~96 K within 15 mins and it can remain cooled for 2 hours by cold nitrogen gas. Alternatively, the sample can be cooled in 60 mins and it can remain cooled for at least 50 hours by LN_2. Slightly higher cooling temperatures could be achieved by using resistive heating instead of the N2 flow or counter-heating , but that is very rarely done. Heating is possible with resistive heating from a filament behind the sample receiver (max. 1200 K), electron-beam heating (max. 1500 K), or direct current heating by treating the sample itself as a resistive element and by sending current through it, as is illustrated in Fig. 5.6b.

Two-dimensional materials, surface alloys, thin films etc. could be synthesised in-situ in the preparation chamber. An evaporation source provided by a user can be added to the preparation chamber without breaking the UHV conditions if it is loaded through a fast entry CF40 port, where a VAT mini gate valve with a CF 16 pumping port and a linear shift mechanism (LSM) are mounted. The source must be short enough to sit behind the closed gate valve when the linear drive is fully retracted. We currently have 100-, 150- and 200-mm travel LSMs available at the beamline. The shortest distance between the source and the sample could be around 50 mm. Furthermore, we have one electron beam evaporator (FOCUS EFM3) that can be made available for users. Users are also welcomed to bring any UHV compatible sources to the SSES. The mounting, pumping, baking and degassing of the sources take about 12 hours. The preparation chamber is equipped with an OCI LEED to characterize crystallised samples and surfaces. It is capable of normal LEED, dynamic I/V curve, and AES measurements. The QMS can be used to analyse the residual gas composition and to perform

Temperature Programmed Desorption (TDS) experiments. The QMS has relatively fast analyse response so that it can follow several masses as a function of time.

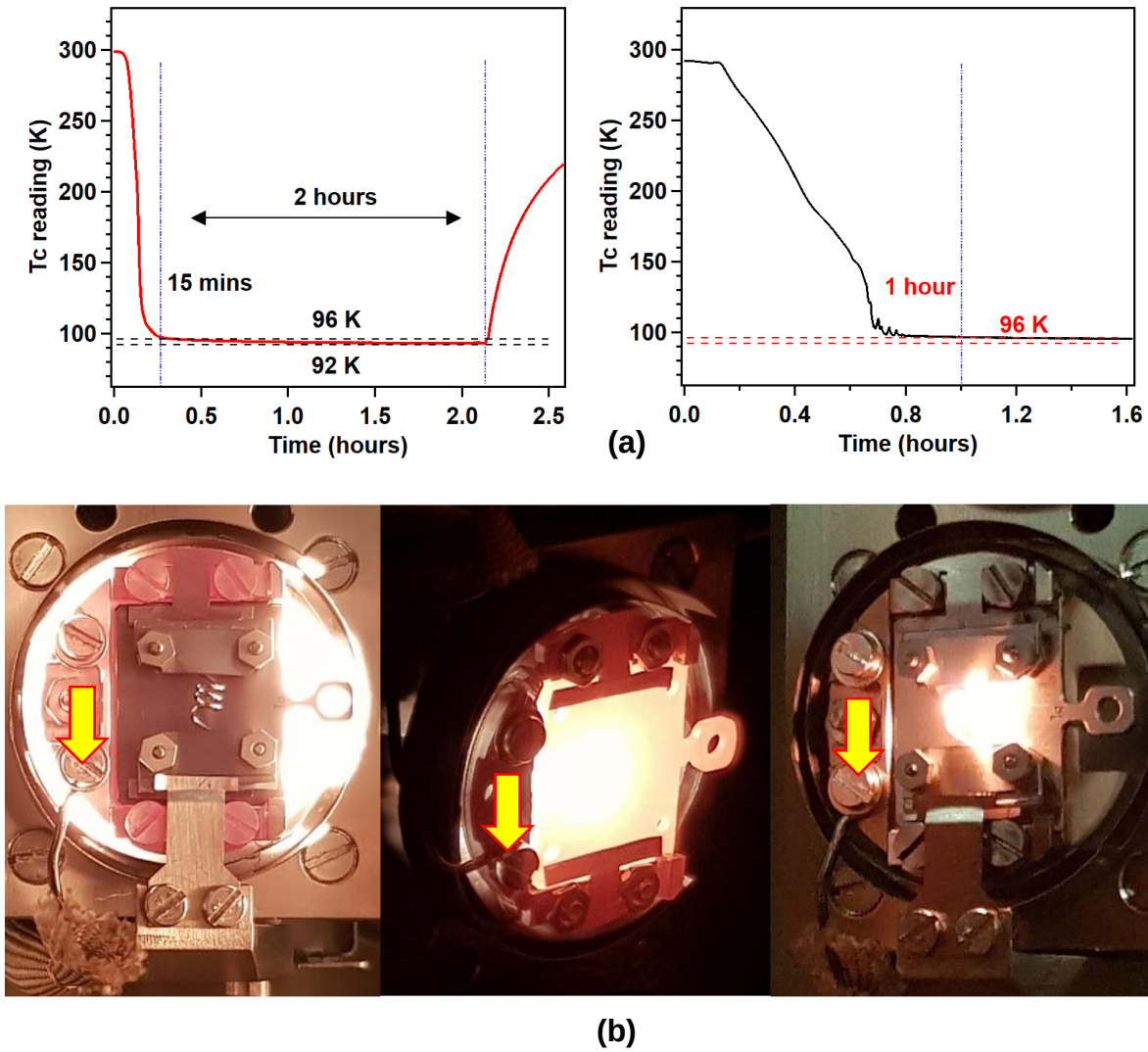

Figure 5.6 *(a) Cooling curves of the resistive heating station measured by a K-type thermocouple mounted at the places pointed by arrows in (b). Two curves were measured under two different setups. The red curve aims at quick but short cooling while the black curve aims at long lasting cooling. (b) Photographs of resistive, e-beam and direct heating.*

5.2 User operation

Thinking about the overall beamline operation at FinEstBeAMS, beamtimes at the SSES are preferably arranged at such times when any major changes to experimental setups are needed at branch A. Since the SSES is permanently installed, users are encouraged to come to MAX IV before the assigned beamtime. The techniques available in the SSES allow users to prepare samples in advance and to perform XPS measurements with an X-ray tube. With the permission of the other users at branch A, it may also be possible to use the photon beam for a short time before the actual beamtime, but this cannot be guaranteed. Furthermore, new users are highly recommended to come before the beamtime for a training in order to be able to work independently, even though most part of the operation at the SSES is accessible by the beamline staff via remote control. The training includes the

control system of the SSES and beamline, sample loading and transferring, troubleshooting when issues arise etc. Users are also welcome to send declared samples to MAX IV with detail information. Beamline staff could load the samples in advance if clear instructions are provided.
A staff member is assigned as a local contact to every beamtime. He (she) is responsible for supervising the experiment during normal working hours, while one person is available for on-call service in evening and weekends. A typical user story could be:

- Sample ready before the beamtime (usually on Wednesday)
- Transfer sample to the pre-defined position in the analysis chamber
- Select proper photon energy and open the beamline
- Align the sample by moving it along the analyser lens axis until maximum count-rate
- Measurement starts

The analyser is controlled by SPECS Prodigy software. Users can set up a programmed plan for overnight measurements. At the SSES, we provide the users with analysis packages for peak fitting, element searching, 1D band structure, and 2D k-space mapping of XPS and ARPES data. During the daytime, a data view and fast-fitting package allow the users to analyse the results immediately. This could help the users to adjust their experimental plan accordingly and to reduce the regrets when analysing data after the beamtime at home. Meanwhile, a second sample could be prepared in the preparation chamber or the load lock. For XAS, total electron yield (drain current) and partial electron yield (Auger or secondary electrons) can be measured simultaneously. A quick data analysing package is under development.

5.3. Issues and solutions

I_0 measurement for XAS

The incident beam flux I_0 is a very important parameter for XAS measurements. One should measure it as close as possible to the sample in order to rule out photon flux losses due to optical elements in the beamline. In the current setting, the closest position where I_0 can be measured is the photocurrent signal of the M4 mirror. However, it is limited by the non-negligible carbon and oxygen contamination of the mirror surface.
The planned solution of this issue is to add between the M4 and the analysis chamber an extra diagnostic chamber, equipped with a gold mesh and an Au evaporator to refresh the mesh regularly. The diagnostic chamber for the measurement of the photocurrent has already been designed within a small (BPAG) project (Fig. 5.7). We have submitted a request (“upkeep process”) to MAX IV management to obtain funding for its acquisition. If funded, the chamber could be ordered straight away and installed some time in 2023.

Partial electron yield (PEY)

The I_0 for PEY is measured by an Alba electrometer controlled by Sardana (the control and data acquisition systems used in MAX IV). However, the analyser is not integrated to Sardana. Hence it is somewhat “tricky” to use I_0 for normalization of the PEY spectra measured by the analyser. The solution is to integrate SPECS Prodigy to Sardana, so that total electron yield and PEY can be programmed and measured simultaneously.

Grating and undulator movement's dead time in XAS measurements

While scanning photon energies for XAS, it typically takes about 80% of time to move the undulator and the monochromator, leaving about 20% of time for data acquisition. The solution is to implement the functionality of continuous scanning (see section 8.3). Based on the experience from FlexPES, it could improve speed of XAS measurements by at least 70%.

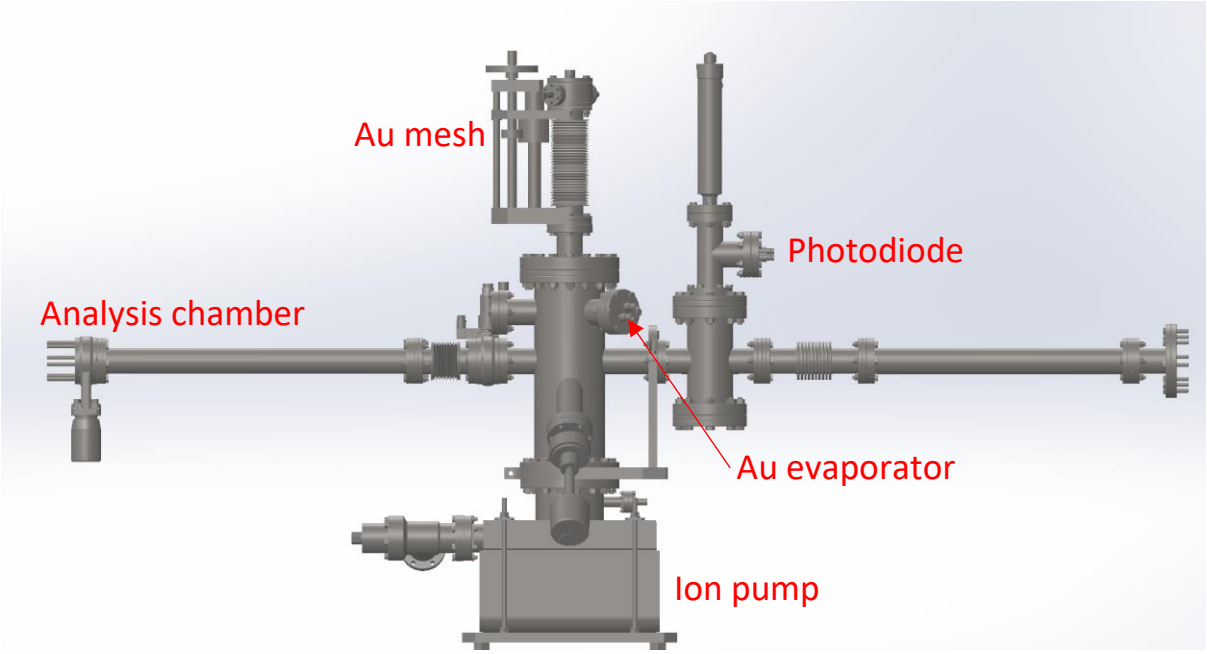

Figure 5.7. *Design of the diagnostic chamber for beam current measurement before the SSES analysis chamber.*

TDS measurement

As mentioned in section 5.1.4, the preparation chamber is equipped with QMS. In order to do TDS properly, we need to integrate QMS control software to Sardana so that it can follow several masses as a function of the thermocouple's input.

Samples stuck in the analyser chamber

The sample receivers in the Ana. and Prep. chambers have very small tolerances for the size of the sample plate, which is not friendly to the users who have their sample mounted in a special way on their own plate. It has already happened several times that the sample plate from another beamline has got stuck in the receiver and the only solution was venting the chamber. A whole week of beamtime could be ruined if that would happen to users. The solution is to ask PREVAC to make an extra prototype of the sample receiver on the analysis manipulator so that we could test the sample plates brought by the users before inserting them into the UHV chamber. However, there would still be no guarantee that it would work since tiny differences could be expected in operation between inside and outside UHV condition.

5.3.1. Issues in the performance of the SPECS analyser

Beam damage on the MCP

Due to the small spot size (~50 µm) in most XPS measurements, only the central part of the detector is often used, resulting in inhomogeneous efficiency across the whole detector. When ARPES is performed, an artificial feature is present as shown in Fig. 5.8. As a temporary solution, flat-field correction can be used to compensate for the inhomogeneity. However, the correction is pass energy and iris size dependent, which means that multiple flatfield corrections are needed to solve this issue and that the correction has to be done manually. Surface Concept (producer of the DLD) explained that the DLD is not designed for ARPES measurements but only for XPS. We are still seeking for a better solution.

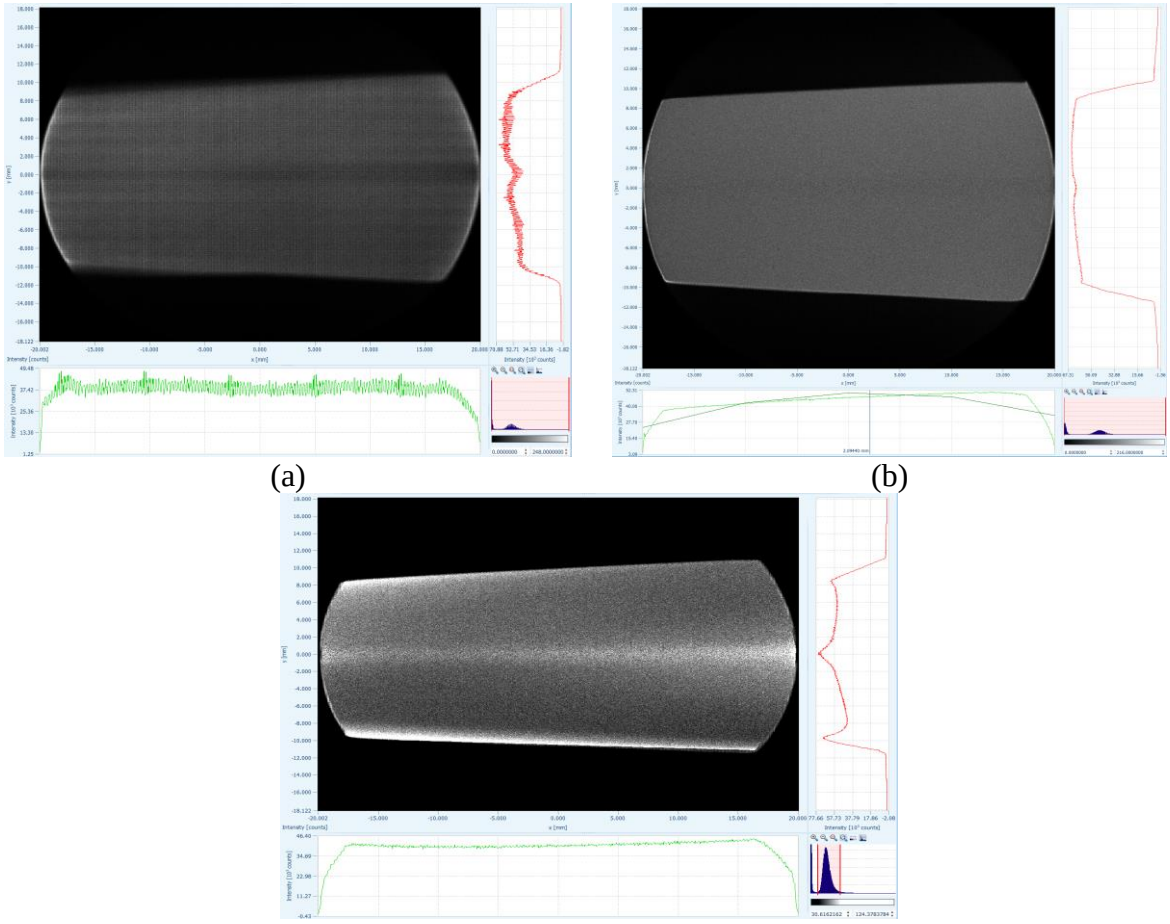

Figure 5.8. *(a) A snapshot image of the detector with WAM lens mode using the pass energy of 10 eV with (b) and without (a) flatfield correction. (c) A snapshot image of the detector taken using the pass energy of 50 eV and with the same flatfield correction as in panel (b), showing artificial overcompensation of the beam damage on the detector.*

Data transformation

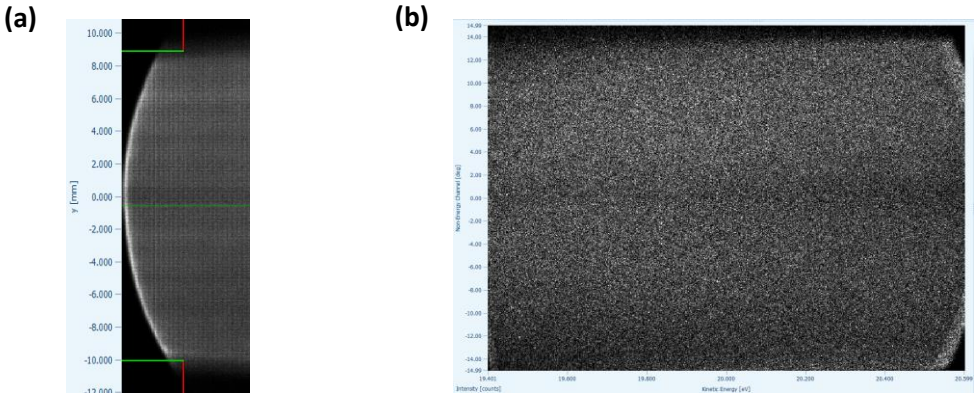

Figure 5.9. *(a) Zoomed area of angular acceptance of figure 5.8 results in asymmetry in transformed data (b) in WAM lens mode.*

An engineer from SPECS claimed that the slight misalignment of the entrance or exit slit shown in Fig. 5.9a should not affect the performance of the analyser, except that we could not achieve full non-energy channel acceptance range as seen in Fig 5.9b. The WAM lens mode should give ±15˚ angular acceptance, but -14˚ to +15˚ is actually detected. By using a defocused X-ray tube to illuminate fully

the detector, we found that the transformation function is also problematic in the sense that it generates an artificial inhomogeneous intensity distribution along the energy axis, see in Fig. 5.10. We have reported this issue to SPECS but they have provided neither solution nor even attention.

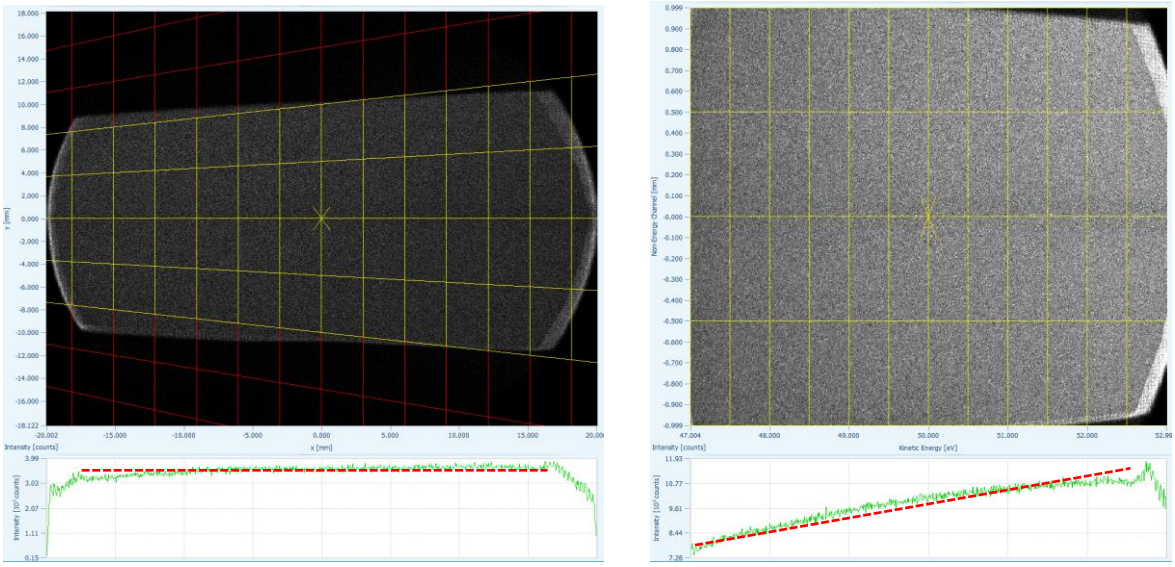

(a) (b)

Figure 5.10. *(a) Raw data and transformed mesh. (b) Transformed data in physical units. The bottom panel shows the intensity profile along the energy axis. The red dashed lines indicate the inhomogeneous intensity distribution.*

Improper lens table for small beam spot

The SPECS analyser has a multi-element transfer lens that can be operated in several modes for angular and spatially resolved studies. Table 5.2 lists the special properties of these modes that were designed for a synchrotron radiation source.

Table 5.2. *Overview of lens modes which are mostly used at the beamline*

	Mode name	property	Application
Angular dispersion mode	High angular dispersion Medium angular dispersion Low angular dispersion Wide angle mode	3.2 mm/° 2.2 mm/° 1.2 mm/° 0.5 mm/°	ARPES Large area UPS
Transmission mode	Large area Medium area Small area	Acceptance area 5 mm Acceptance area 2 mm Acceptance area 0.1 mm	XPS/UPS of different spot sizes of the source
Acceleration mode	High magnification 2	Magnification: 10	Optimized for low kinetic energy (<100 eV)

However, except for Angular dispersion mode, no other lens mode could focus the beam properly on the detector as shown in Fig. 5.11.

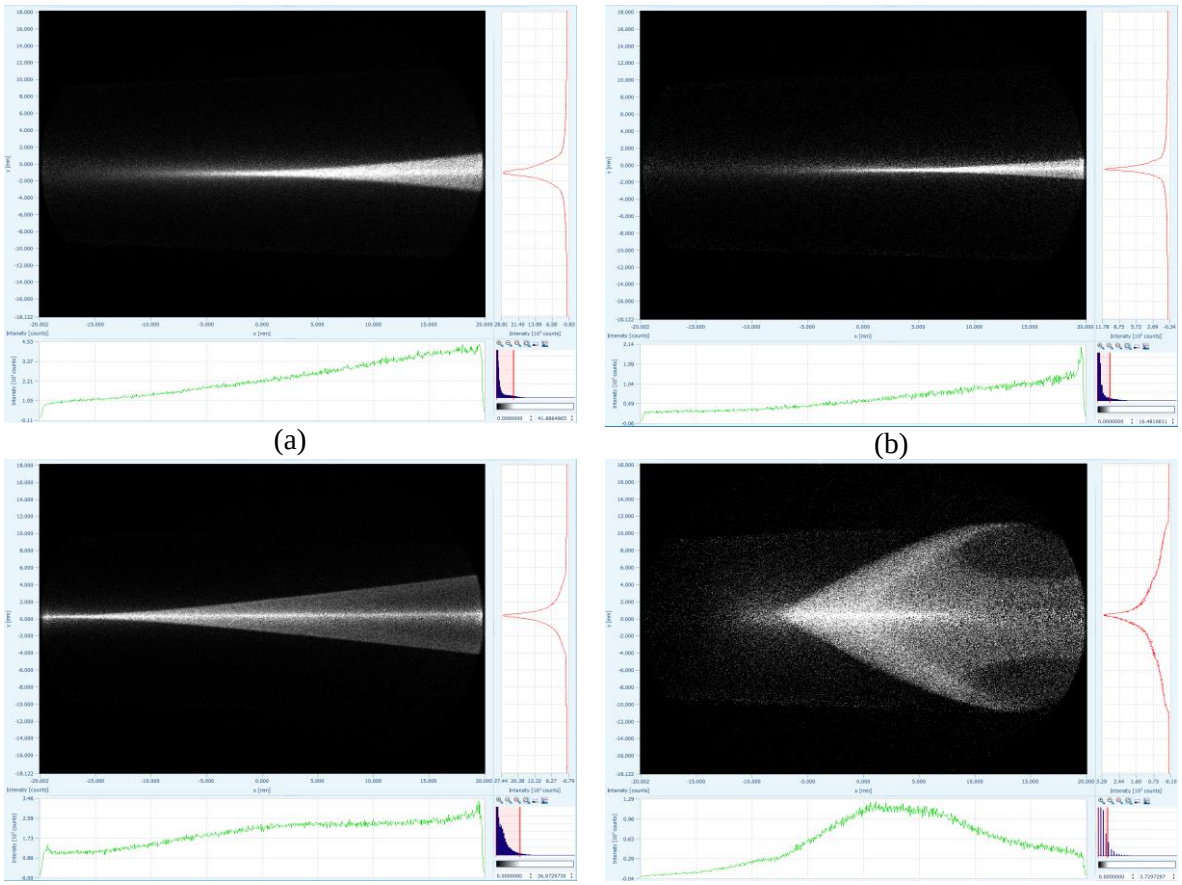

Figure 5.11. *Snapshot images obtained with different lens modes (a) HM2, (b) LA, (c) MA, and (d) SA. The photon energy was 200 eV, retarding ratio: 1. The working distance was optimized by maximizing cps.*

Misalignment of analyser slits

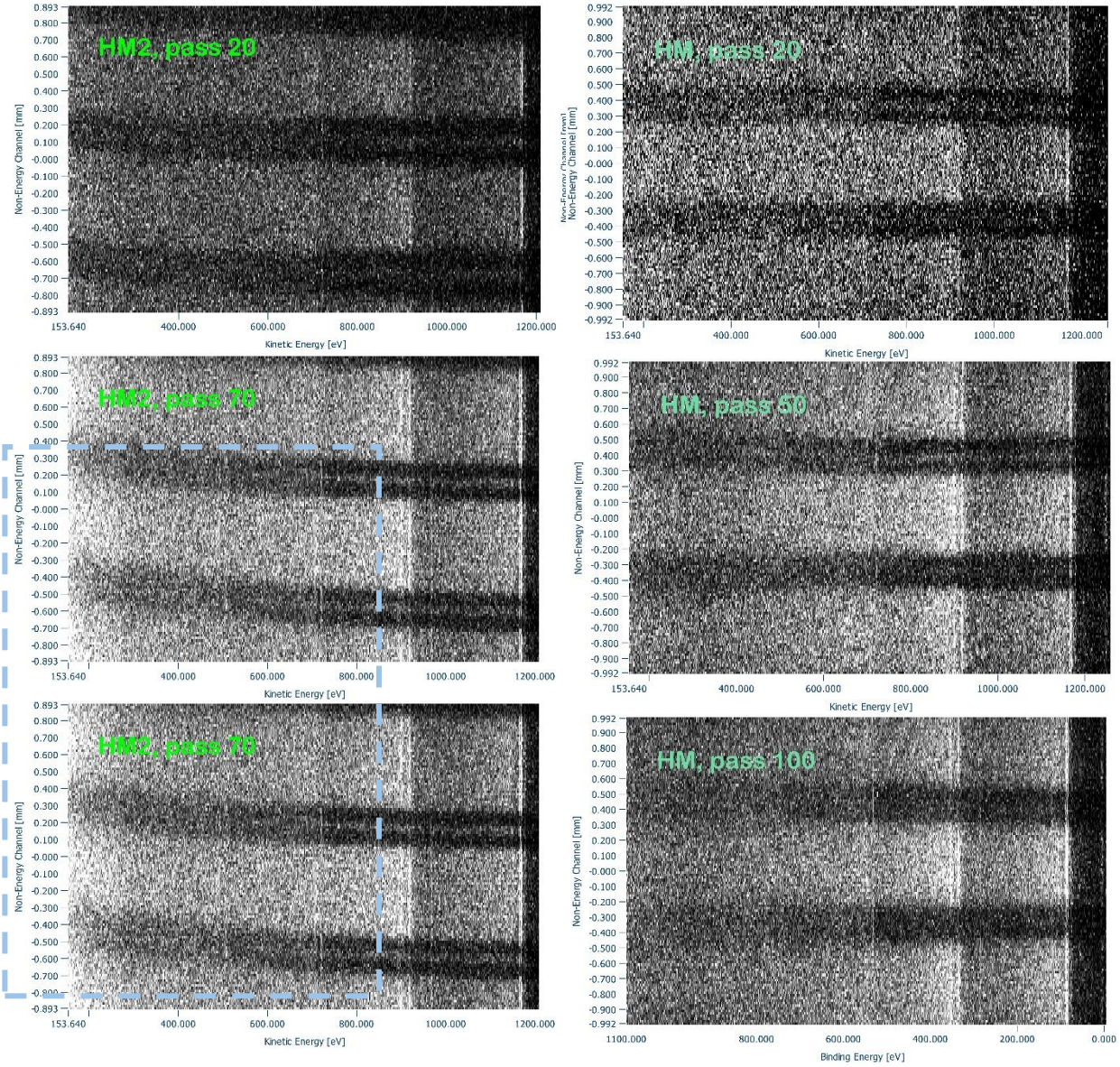

Figure 5.12. *Survey scan XPS using 'High Magnification 2' (HM2) and 'High Magnification' (HM) lens modes, at different pass energy values (in eV) as labelled, from a patterned gold sample on Si substrate (period ~0.7 mm, of which the gold patch is ~0.5 mm wide; Au 4f and 4d lines visible), measured using wide illumination Mg-Ka excitation from x-ray gun. On the spectrometer, the 0.8x20mm2 (curved) analyser entrance slit was used, and iris diameter was set to 10 mm. The dashed line blue frame emphasizes the indication of off-lens-axis analyser entrance slit.*

We take this upward turning curves (at lower kinetic energies in the images presented in the figure 5.12) as an indication that apart from the lens tables falling short of maintaining appropriate focusing conditions throughout a wider kinetic energy range, the analyser entrance slit is also significantly geometrically offset from a position where it would be positioned symmetrically with respect to the lens axis. We would think that since the radial distribution within the lens peaks at the axis, the physical adjusting of the entrance slit might improve the overall transmission, which for higher excitation energies is quite relevant.

5.4. Comparison with similar end stations

There are many XPS/XAS end stations located at synchrotron radiation facilities in Europe. The SSES together with all other end stations at MAX IV have the advantage of the world's first forth-generation storage ring. Since there are too many competitors in this game, we enumerate only two similar multi-functional endstations in table 5.3. SuperESCA is the predecessor of multi-functional end stations that perform PES and XAS experiment. BACH is a good example for future development of new techniques at the SSES. In a short summary of this comparison, we would like to highlight two aspects. One is the lowest photon energy, the other is the full control of beam polarization.

Table 5.3. *Comparison of characteristics of the SSES with two end stations at Elettra.*

	SSES at FinEstBeAMS	SuperESCA at Elettra	BACH at Elettra
Years of operation	2021-	1994-	2001-
Monochromator	cPGM	SX700 PGM	VASGM
Photon energy range	G2: **4.5** – 50 eV G1: 15 – 800 (1300) eV	90 - 1800 eV	SG1 44 eV-349 eV SG2 158 eV-597 eV SG3 491 eV-1600 eV SG4 301 eV-1600 eV
Polarization	Linear H, V In progress: inclined, circular (11-200 eV)	Linear H	Linear H, V Circular
Resolving power (R)	5000 (12.89 eV with G2) 18400 (21.59 eV with G1) 11000 (400 eV)	10000 (400 eV) 5000 (900 eV)	12000 (90 eV) 6600 (867 eV)
Photon flux	10^{13} photon/s @ 100 eV	10^{13} photon/s @ 200 eV	>10^{13} photons/s
Spot size on sample	(50-150)(H)×20(V) μm^2	(100-150)(H) × (5-100)(V) μm^2	(250-350)(H) × (10-350)(V) μm^2
Sample manipulation	5 axis manipulator with LN2 cryostat with possibility of LHe cooling (under commissioning)	2 manipulators: 4 axis manipulator with LHe cryostat 5 axis manipulator with LN2 cryostat	2 manipulators: 4 axis manipulator with LHe cryostat 5 axis manipulator with LN2 cryostat
Sample environment	92 – 500K	120-1500K; 15-1500K	110-1300K; 50-1300K
Analyzer and detector	SPECS Phoibos 150 R7 + 2D DLD	SPECS Phoibos 150 R7 + 1D DLD	Scienta3000, ComIXS fluorescence spectrometer, Channeltron and MCP, Ultrafast MCP
Experimental techniques	XPS, TEY-XAS, PEY-XAS, ARPES, LEED, AES, TDS	NEXAFS, ARPES, PED, time-resolved XPS, LEED	ARPES, TEY-XAS, PEY-XAS, total and partial fluorescence yield, XMCD, X-ray emission spectroscopy, LEED

5.5. Future development and commissioning projects

The projects are presented in the sequence of priority.

1. **Diagnostic chamber for I_0**

The motivation has been described in section 5.3.

2. **UV lamp and XRF detector (ongoing)**

There are three end stations at the FinEstBeAMS beamline, meaning that more than half of the beamtime is not available to the SSES's users. Hence, we plan to install an UV lamp to enhance the use of the SSES. Together with an X-ray tube, we could provide more power for off-line experiments by offering both low and high photon energies. Furthermore, we plan to add an X-Ray Fluorescence (XRF) detector to implement the capability of XAS measurements on insulating samples. The negotiation of purchasing an UV lamp and an XRF detector is ongoing between the FinEstBeAMS team and an Estonian research group.

3. “Dirty” preparation chamber

End stations at various beamlines are working mostly in UHV conditions, which limits the sample synthesizing method. There is a fair number of users, willing to do in-situ measurements, but their sample preparation would contaminate the UHV chamber or devices. Therefore, a movable “dirty” sample preparation chamber would open a possibility for those users to perform experiments at FinEstBeAMS and other beamlines at MAX IV. The word “dirty” could mean different methods of sample synthesis, such as PVD, CVD or ALD. A good example could be the LOREA beamline at ALBA. The chamber should be very compact so that it could fit into different designs of the main UHV chambers at the different beamlines at MAX IV.

5.6. Specific questions for SSES

1. Does the committee agree that the issues outlined in section 5.3 could be solved with the solutions presented? Are there alternative solutions that could be better?
2. Does the committee agree with the priority of the future development and commissioning projects for SSES outlined in section 5.5?
3. What is the best path to develop the SSES? There are two scenarios. One is to expand the concept of “multi-functionality”, i.e., to develop the characteristics of current techniques and implement new techniques, e.g., photoluminescence, in a balanced way. The other possibility is to emphasize the performance of one specific technique.

6. Beamline operation

6.1. Categories of beamtime

MAX IV gives the following guideline (Table 6.1) to beamlines in regular user operation on how available beamtime should be divided between different categories or purposes that are explained more in detail below the table.

Table 6.1. *MAX IV guideline for division of beamtime.*

Category	Guideline
General users	60-75%
from which Fast access	≤ 20%
Training & Education	2%
Proprietary ("industrial users")	≤ 20%
In-house research and commissioning, maintenance	20-25%

General users. Scientists who want to perform experiments at MAX IV Laboratory submit beamtime proposals in proposal calls that are open twice a year. The proposal calls of 2022 were arranged in February-March and in September. Review panels composed of external experts evaluate the proposals, rank them and suggest which proposals should be granted with beamtime and with how many shifts (one shift is 4 h*)*. MAX IV management makes the final decision on approved proposals based on the recommendations of the review panels. FinEstBeAMS participates in these regular user calls. As FinEstBeAMS has three different research directions (surface science, photoluminescence and gas-phase or low-density matter research), beamtime proposals submitted to FinEstBeAMS are divided to three different review panels. It would be difficult to compare the proposals of different research directions with each other, and it is not done presently. Instead, the number of approved proposals (or shifts) for each end stations has depended on the number of proposals (or shifts) submitted to each end station in a particular user call. However, there is no formal decision on how beamtimes at FinEstBeAMS should be divided between the end stations. Thus, it would be possible to set later predetermined beamtime quotas for the different end stations if one of them began to receive much more (or less) beamtime proposals than the other two.

Fast access. Citing a MAX IV web page on proposal types, "MAX IV offers access on short notice, for a limited amount of shifts, to experiments that require timely access to our facility". FinEstBeAMS staff have decided to accept fast access proposals for the first time in the spring 2023 call, but only for the SSES. Users can submit fast-access proposals also outside normal user calls. The maximum allowed beamtime for a fast access proposal will be six shifts (1 day).

Training & education. In regular proposal calls, users can submit beamtime proposals that focus on training or education of participants such as university students or upper secondary school teachers. A review panel will evaluate submitted T&E proposals.

Proprietary. Industrial users can apply for beamtime at MAX IV through industry-privileged proprietary access. These beamtimes are mediated via MAX IV Industrial Relations Office. FinEstBeAMS has not hosted any proprietary beamtimes so far.

In-house research and commissioning, maintenance. *In-house research* intends research aiming at publications carried out by the beamline staff itself, but it can be done in collaboration with external research groups. At FinEstBeAMS, postdoctoral researchers are principal recipients of in-house research beamtime because they are expected to get publications during their limited working periods at the beamline (presently 2 years, but soon extendable by one more year). A FinEstBeAMS post-doc typically receives one week of beamtime per semester. Depending on beamtime availability, other beamline staff members have also received 2-5 days of in-house research beamtime per semester.

During *in-house commissioning* beamtimes, the beamline staff typically tests functionality of the beamline or characterizes one of the beamline instruments such as an electron spectrometer. Such a use of beamtime does not usually aim at collecting data for publications. In-house research and commissioning beamtimes are granted via simplified proposals, where an applicant sends the title and brief description of the experiments to be performed to the beamline manager, who adds an in-house proposal in the beamtime calendar. Maintenance [of the beamline and its instrumentation] is quite similar to in-house commissioning. They could be distinguished by that maintenance activity does not use the photon beam, but it can prevent its use for other purposes.

Expert commissioning involves commissioning of the beamlines' instruments by other persons than the beamline staff, but, in practice, it is often done in collaboration between the beamline personnel and external scientists. Beamlines can specifically reserve beamtime for that purpose, and it is typically done at the initial stages of the beamline's development, i.e., before the beamline enters normal user operation. Expert commissioning can also be given when a new setup is being developed for the beamline and experience from its use by external experts could be used to finalize the setup.

6.2. Use of beamtime and proposal statistics

FinEstBeAMS received first light in the front end on 24 November 2017 and at the end station (GPES) on 23 April 2018. There was a delay of six weeks in January-February 2018 in commissioning of FinEstBeAMS because the beamline's radiation permit was temporarily withdrawn. The first test experiments at FinEstBeAMS were performed in May 2018. A commissioning call for the GPES and PLES ("C_HT18" in Table 3.2) was opened in June 2018. A specific proposal call for FinEstBeAMS was arranged in 2019 ("FE_VT19" in Table 3.2). Regular user operation begun in April 2019. FinEstBeAMS has participated in regular MAX IV proposal calls since the HT19 call. Table 6.2 summarizes submitted and scheduled proposals per proposal call. It also denotes the splitting of beamtimes between the three end stations of FinEstBeAMS.

Table 6.2. *History of submitted and scheduled proposals at FinEstBeAMS. Included are general user, commissioning expert, and training & educational proposals. The numbers in parentheses denote the numbers of scheduled shifts (one shift is 4 h).*

	C_HT18	FE_VT19	HT19	VT20	HT20	VT/HT21	VT22	Fall22
Submitted	8*	20	22+2*	16	14	19	19+1^{o}	20+1^{o}
Scheduled	7*	9	10+2*	7	11	7	12+1^{o}	11+1^{o}
- GPES	5* (162)	5 (150)	6+1* (210)	3 (90)	5 (150)	3 (90)	8 (240)	3+1^{o} (90+30)
- PLES	2* (60)	4 (90)	4+1* (150)	4 (120)	5 (150)	2 (60)	3 (90)	3 (78)
- SSES					1 (30)**	2 (60)	1+1^{o} (30+2)	5 (138)

* indicates commissioning experts, ^{o} indicates T&E, ** transferred from FlexPES,

The list of originally accepted proposals is in some cases different from the list of scheduled proposals because some users have had to cancel their proposals, most often due to Covid-19. A cancelled proposal may have been replaced by another proposal in the reserve list or, when that has not been possible, by in-house research or in-house commissioning. During the Covid-19 pandemic, the experiments of many proposals were performed outside of their proper semesters. As was already mentioned in Introduction, FinEstBeAMS was completely closed in spring 2021 due to the Covid-19 pandemic. In fall 2021, FinEstBeAMS rescheduled nine previously cancelled beamtimes from the HT20 call, while the proposals from the merged VT/HT21 proposal call were placed in the reserve list. At the end, seven of the proposals from the merged VT/HT21 call could be scheduled. Starting from the proposal call VT22, the scheduling of the proposals has returned to its natural cycle in the sense that there were no longer proposals to be rescheduled due to Covid-19.

Nationality. Neglecting a short T&E proposal of two shifts, 76 beamtime proposals have been scheduled at FinEstBeAMS. Several proposals have participants from more than one country, hence dividing them between countries is a little artificial. Nevertheless, the principal investigators of the scheduled proposals have had their home institutes in the following countries: Estonia 25 (33%), Finland 12 (16%), Russia 9 (12%), Latvia 7 (9%), Sweden 7 (9%), Germany 4 (5%), France 3 (4%), United Kingdom 3 (4%), Norway 3 (4%), others 3 (4%).

Recurring users. The user community of FinEstBeAMS has been characterized by users that have performed earlier experiments at the beamline. Starting from the first general MAX IV user call, in which FinEstBeAMS participated, the share of recurring users can be considered to have been as follows: six of 12 proposals (50%) in HT19, five of seven proposals (71%) in VT20, eight of 11 proposals (73%) in HT20, three of seven proposals (43%) in VT/HT21, 11 of 12 proposals (92%) in VT22, and seven of 12 proposals (58%) in Fall22. The somewhat lower shares in the VT/HT21 and Fall22 calls reflect the influx of new users to the solid-state end station.

Table 6.3 reports how beamtime at FinEstBeAMS has been used for different purposes in the years 2019-2022. We have made the calculation over calendar years because rescheduling of beamtimes in 2020-2021 moved proposals away from their own semesters. So-called friendly users already performed five commissioning experiments at FinEstBeAMS in autumn 2018. Those users came from the Finnish and Estonian research groups that had strongly contributed to the building of the beamline or to the development of its end stations. Systematic scheduling of beamtimes was started with the approved proposals of the commissioning experts at the beginning of 2019 (one of those experiments took place in 2018). Normal user operation begun in April 2019 at the GPES and few weeks later at the PLES. In 2020, the beamtimes of many users were cancelled due to Covid-19 in 2020, but the MAX IV staff could work at the laboratory. Consequently, more beamtime was used for commissioning of the beamline and its end stations than would have been possible under normal conditions. For instance, the GPES was completely removed from the beamline in summer 2020 and a MAX IV polarimeter was mounted at its place to characterize the polarization properties of monochromatized radiation at the sample position.

Table 6.3. *Use of beamtime in weeks at FinEstBeAMS calculated in the years 2019-2022. The following abbreviations are used: G = gas-phase end station, P = photoluminescence end station, S = solid-state end station, Pol = polarimeter, Mono = monochromator, SB = single-bunch operation.*

	2019	**2020**	**2021**	**2022***
General Users	16 (G 9, P 7)	8 (G 5, P 3)	14 (G 7, P 6, S 1)	26.5^{o} (G 12^{o}, P 7, S 7.5)
Expert commissioning	6 (G 4, P 2)	2 (SB: G 1, P 1)	-	-
In-house commissioning	6 (Mono 3)	11.5 (S 2.5, Pol 3, P 2)	3	1.5
In-house research	5	9.5 (P 5, G 2.5, S 2)	3.5	6.5
Maintenance	1	1	-	-
Lost beamtime			14	
Total	34	32	20.5	34.5
Share of general users	47%	24%	68%	77%

*projected, ^{o}includes one week of T&E beamtime

FinEstBeAMS was closed for a long time in spring 2021. Even the FinEstBeAMS staff were not allowed to work at the beamline. Fourteen weeks of beamtime were lost. When the beamline was finally opened, external users and visitors were not allowed at the laboratory until 13 September 2021, and any user experiments before that date had to be performed by the MAX IV staff. The PLES has had a strong Russian user community. Our Russian users continued to suffer from a travel ban from Russia to Sweden even when users from EU could arrive at MAX IV for their experiments. As a result, Kirill Chernenko carried out measurements for four of the six proposals that were executed at the PLES in

2021. The measurement programs had to be condensed for such beamtimes because one man could not work so long at the beamline as a whole team could have done. The year 2022 can be considered the first almost normal year since the beginning of user operation at FinEstBeAMS. We write *almost* because the ongoing war between Russia and Ukraine has also affected user operation of FinEstBeAMS. One approved proposal of a Russian PI was cancelled in spring 2022 as a sanction against Russia. Presently, users having Russian affiliations cannot submit beamtime proposals to FinEstBeAMS or to other beamlines at MAX IV.
If there are no further unexpected events, FinEstBeAMS will achieve the goal of offering 70-75% of available beamtime to general users in 2022.

6.3. User feedback

Using grades (1-5), the users can give feedback in DUO about their beamtimes in the following categories: facility, beamline, user support, and overall success. In addition, they can leave written comments about the same categories. It is quite tedious to analyse the numerical values because general proposals are mixed with in-house proposals (which may be less objective and are not considered here), many users of the same beamtime can leave their grades, and the feedback items appear in a large table in the time order when feedback was submitted. It would be possible to carry out an analysis of the user feedback in the end station level because an experimental proposal number is attached to each feedback item. We do not give such results because the numbers of evaluated beamtimes have been rather small. Instead, Table 6.4 summarizes the results of user feedbak in different years. The numbers have been extracted by counting firstly the average scores for each proposal in four categories, and secondly the averages between the average scores of the different proposals. Thus, each evaluated beamtime has the same weight for the final scores of that year.

Table 6.4. *The average grades of the general users' evaluations of their beamtimes at FinEstBeAMS in the years 2019-2022.*

	2019	**2020**	**2021**	**2022**
Facility	4.29	4.27	4.48	4.46
Beamline + end station	4.12	4.34	4.27	4.25
User support	4.61	4.78	4.61	4.36
Overall success	4.28	4.31	4.58	4.27
# Evaluated beamtimes	24	10	9	9

In general, the users seem to have been quite happy with their beamtimes at FinEstBeAMS. However, we note that there has been a decrease in the appreciation of user support and overall success in the year 2022. This was due to unhappy circumstances when the local contact of two beamtimes became ill of Covid-19 and the other FinEstBeAMS team members could not help the users nearly so well. This incident highlights a weakness in staffing at FinEstBeAMS. Each permanent staff member is specialized in one end station only. Should any of them become incapable of working due to an illness or an accident, it would be difficult to arrange adequate user support for experiments at that particular end station.
We can also observe that the users give now less feedback than at the beginning of user operation. They may have become tired of filling those forms after each beamtime or they may think that their earlier responses have not led to any improvements.

6.4. Publications

As of 6 September 2022, we are aware of 38 publications that are somehow connected to FinEstBeAMS. In the following publication list, we do not report manuscripts that have been accepted for publication but are not yet published, except for the manuscript about the SSES (publication 6). The

publications are divided in four sub-categories (instrumentation, gas-phase research, photoluminescence research, and surface science) according to the main purpose of the works.

Publications about instrumentation (6):

1. R. Pärna *et al*., "FinEstBeaMS – A wide-range Finnish-Estonian beamline for materials science at the 1.5 GeV storage ring at the MAX IV Laboratory", Nucl. Instrum. Methods Phys. Res. A 859, 83-89 (2017).
2. V. Pankratov *et al*., "Progress in development of a new luminescence setup at the FinEstBeAMS beamline of the MAX IV Laboratory", Radiat. Meas. 121, 91-98 (2019).
3. P. Sjöblom, G. Todorescu, and S. Urpelainen, "Understanding the mechanical limitations of the performance of soft X-ray monochromators at MAX IV laboratory, J. Synchrotron Rad. 27, 272-283 (2020).
4. K. Kooser *et al*., "Gas-phase endstation of electron, ion and coincidence spectroscopies for diluted samples at the FinEstBeAMS beamline of the MAX IV 1.5 GeV storage ring", J. Synchrotron Rad. 27, 1080-1091 (2020).
5. K. Chernenko *et al*., "Performance and characterization of the FinEstBeAMS beamline at the MAX IV Laboratory", J. Synchrotron Rad. 28, 1620-1630 (2021).
6. W. Wang *et al*., "A new user-friendly materials science end station at the FinEstBeAMS beamline of MAX IV", Proceedings of the SRI-2021 Conference, to be published in J. Phys. Conf. Series.

Publications about gas-phase research (11):

7. I. Kuusik *et al*., "The electronic structure of ionic liquids based on the TFSI anion: A gas phase UPS and DFT study", J. Mol. Liq. 294, 111580 (5 pp) (2019).
8. A.R. Abid *et al*., "Electron-ion coincidence spectroscopy of a large organic molecule: photofragmentation of avobenzone after valence and core ionisation", J. Phys. B: At. Mol. Opt. Phys. 53, 244001 (12 p) (2020).
9. E. Pelimanni *et al*., "Core and valence level photoelectron spectroscopy of nanosolvated KCl", J. Phys. Chem. A 125, 4750-4759 (2021).
10. I. Kuusik *et al*., "Ionic liquid vapors in vacuum: possibility to derive anodic stabilities from DFT and UPS", ACS Omega 6, 5255-5265 (2021).
11. J. Kruusma *et al*., "The electrochemical behaviour of protic quaternary amine based room-temperature ionic liquid N2210(OTf) at negatively and positively polarized micro-mesoporous carbon electrode investigated by in situ X-ray photoelectron spectroscopy, in situ mass-spectroscopy, cyclic voltammetry and electrochemical impedance spectroscopy methods", J. Electroanal. Chem. 897, 115561 (11 pp) (2021).
12. J. Kruusma *et al*., "The electrochemical behaviour of quaternary amine-based room-temperature ionic liquid N4111(TFSI)", Catalysts 11, 1315 (24 pp) (2021).
13. M. Patanen *et al*., "Valence shell photoelectron angular distributions and vibrationally resolved spectra of imidazole: A combined experimental-theoretical study", J. Chem. Phys. 155, 054304 (16 pp) (2021).
14. L. Pihlava *et al*., "Photodissociation dynamics of halogenated aromatic molecules: the case of core-ionized tetrabromothiophene", Phys. Chem. Chem. Phys. 23, 21249-21261 (2021).
15. M. Kook *et al*., "Ion fragmentation study of [EMMIM]\[TFSI], [EMIM][OTf] and [EMIM][DCA] by vacuum ultraviolet light", Int. J. Mass Spectrom. 471, 116732 (8 pp) (2022).
16. O. Travnikova *et al*., "Ultrafast dissociation of ammonia: Auger Doppler effect and redistribution of the internal energy", Phys. Chem. Chem. Phys. 24, 5842-5854 (2022).
17. M.D. Kiselev *et al*., "An experimental and theoretical study of the Kr 3d correlation satellites", J. Phys. B: At. Mol. Opt. Phys. 55, 055002 (15 p) (2022).

Publications about photoluminescence research (21):

18. A.P. Kozlova *et al*., "Low-temperature luminescence of catangasite single crystals under excitation by vacuum ultraviolet synchrotron radiation", Low Temp. Phys. 46, 1178-1184 (2020).
19. V. Pankratova *et al*., "Time-resolved luminescence and excitation spectroscopy of Co-doped $Gd_3Ga_3Al_2O_{12}$ scintillating crystals", Sci. Rep. 10, 20388 (11 p) (2020).
20. A. Kaminska *et al*., "Defect-related photoluminescence and photoluminescence excitation as a method to study the excitonic bandgap of AlN epitaxial layers: Experimental and *ab initio* analysis", Appl. Phys. Lett. 117, 232101 (6 pp) (2020).
21. I. Kamenskikh *et al*., "Decay kinetics of CeF_3 under VUC and X-ray synchrotron radiation", Symmetry 12, 914 (12 pp) (2020).
22. A.P. Kozlova *et al*., "Luminescence and vacuum ultraviolet excitation spectroscopy of cerium doped $Gd_3Ga_3Al_2O_{12}$ single crystalline scintillators under synchrotron radiation excitations", Results Phys. 16, 03002 (6 pp) (2020).
23. V. Pankratov and A. Kotlov, "Luminescence spectroscopy under synchrotron radiation: From SUPERLUMI to FINESTLUMI", Nucl. Instrum. Meth. Phys. Res. B 474, 35-40 (2020).
24. D. Spasskiy *et al*., "Enhancement of light output in $Sc_xY_{1-x}PO_4:Eu^{3+}$ solid solutions", Symmetry 12, 946 (9 pp) (2020).
25. D. Spasskiy *et al*., "Influence of Sc cation substituent on structural properties and energy transfer processes in GAGG:Ce crystals", CrystEngComm 22, 2621 (11 pp) (2020).
26. A. Shalaev *et al*., "Luminescence of divalent lanthanide doped BaBrI single crystals under synchrotron radiation excitations", Nucl. Instrum. Meth. Phys. Res. B 467, 17-20 (2020).
27. V. Pankratova, P. Juris, and V. Pankratov, "Low-temperature luminescence of ScF_3 single crystals under excitation by VUV synchrotron radiation", Low Temp. Phys. 46, 1196-1200 (2020).
28. E. Trofimova *et al*., "Luminescence properties and energy transfer processes in $LiSrPO_4$ doped with Pr^{3+} and co-doped with Na^+ and Mg^{2+}", J. Lumin. 240, 118455 (9 pp) (2021).
29. J. Saaring *et al*., "Relaxation of electronic excitations in K_2GeF_6 studied by means of time-resolved luminescence spectroscopy under VUV and pulsed electron beam excitation", J. Alloys Compd. 883, 160916 (11 pp) (2021).
30. A. Vanetsev *et al*., "Microwave-hydrothermal synthesis and investigation of Mn-doped K_2SiF_6 microsize powder as a red phosphor for warm white LEDs", J. Lumin. 239, 118389 (10 pp) (2021).
31. V. Khanin *et al*., "Exciton interaction with Ce^{3+} and Ce^{4+} ions in $(LuGd)_3(Ga,Al)_5O_{12}$ ceramics, J. Lumin. 237, 118150 (6 pp) (2021).
32. S. Gundacker *et al*., "Vacuum ultraviolet silicon photomultipliers applied to BaF_2 cross-luminescence detection for high-rate ultrafast timing applications", Phys. Med. Biol. 66, 114002 (18 pp) (2021).
33. D. Spasskiy *et al*., "Structural, optical and luminescent properties of undoped $Gd_3Al_xGa_{5-x}O_{12}$ (x=0,1,2,3) and $Gd_2YAl_2Ga_3O_{12}$ single crystals", Opt. Mater. 125, 112079 (10 pp) (2022).
34. T. Garmysheva *et al*., "Luminescence of ODC(II) in quartz and cristobalite glasses", J. Non-Cryst. Solids 575, 121199 (7 pp) (2022).
35. J. Kappelhoff *et al.*, "Spectroscopic studies on Pr^{3+} doped YPO_4 and $LuPO_4$ upon vacuum ultraviolet (VUV) and synchrotron radiation excitation", Chem. Phys. 562, 111646 (9 pp) (2022).
36. J. Saaring *et al*., "Time-resolved luminescence spectroscopy of ultrafast emissions in $BaGeF_6$", J. Lumin. 244, 118729 (9 pp) (2022).
37. R.E. Rojas-Hernandez *et al*., "Deep-Ultraviolet Emitter: Rare-Earth-Free $ZnAl_2O_4$ Nanofibers via a Simple Wet Chemical Route", Inorg. Chem. 61, 11886-11896 (2022).
38. R. Assylbayev *et al*., "Defect-related luminescence of MgO single crystals irradiated with swift ^{132}Xe ions", Opt. Mater. 127, 112308 (7 pp) (2022).

Publications about surface science (1):

39. L. Palmolahti *et al*., "Pinhole-resistant nanocrystalline rutile TiO_2 photoelectrode coatings", Acta Mater. 239, 118257 (9 pp) (2022).

We can see that photoluminescence users have published almost twice as many articles as gas-phase users, even though they have had fewer beamtimes (Table 6.3). As there were 19 general user and commissioning expert beamtimes at the PLES in 2019-2021, one can conclude (rather boldly) that the photoluminescence users have managed to publish the results of their measurements on average within one year of their beamtimes. In gas-phase synchrotron radiation research at FinEstBeAMS (and elsewhere), an average time between experiments and publication seems to be clearly longer.
Research articles from FinEstBeAMS have mostly been published in the journals of specialized research fields, the clearest exception being Scientific Reports (publication 19). Acta Materialia that published the first surface science study (39) from FinEstBeAMS has by far the highest impact factor (9.209). The impact factors of the journals that have published the above-listed gas-phase and photoluminescence studies range from 0.923 to 5.436, whereby the highest value belongs to Inorganic Chemistry (publication 37). The average impact factor for FinEstBeAMS publications in gas-phase research is 3.33 and that in photoluminescence research is practically identical, 3.21. Articles about instrumentation (1-6) were not included in the above considerations about impact factors.

6.5. Staffing

The FinEstBeAMS team currently consists of one permanently employed beamline scientist, two permanently employed research engineers, one postdoc employed by MAX IV, one postdoc employed by Lund University's Faculty of Engineering, one temporary guest researcher, and an externally funded postdoc, who very recently joined the team. These persons are introduced below.
Antti Kivimäki (scientist, permanent). In 2016-2021, Antti was employed as a senior research fellow by the University of Oulu, but he worked full-time at FinEstBeAMS. He obtained a beamline scientist position at MAX IV in 2021. He works as the beamline manager of FinEstBeAMS. He is responsible for the GPES, participates in user support and has local contact duties at the GPES.
Kirill Chernenko (research engineer, permanent). Kirill was hired as a postdoc at FinEstBeAMS in 2018. He obtained the position of a research engineer in 2020. Kirill carries the main responsibility for keeping the beamline in operation. He is responsible for the PLES, participates in user support and has local contact duties at the PLES. He also helps in most diverse other tasks at FinEstBeAMS.
Weimin Wang (research engineer, permanent). Weimin was hired in his present position at FinEstBeAMS in 2019. He has worked previously as a scientist at Bloch in 2018-2019. Weimin is responsible for the SSES – the most complicated of the FinEstBeAMS end stations – and for the B branch of FinEstBeAMS. He participates in user support and has local contact duties at the SSES.
Calle Preger (LTH postdoc in aerosol science, temporary). Calle's postdoc position, which begun in February 2021, is funded through collaboration between the Faculty of Engineering (LTH) at Lund University and MAX IV. Calle's main task has been the development and commissioning of an aerosol delivery system.
Amirreza Ghassami (MAX IV postdoc in surface science, temporary). Amirreza's postdoc position started in November 2021. He carries out research using the SSES and the STM laboratory. He participates in maintenance and development of the SSES.
Tanel Käämbre (guest researcher, temporary). Tanel has long experience in both gas-phase and surface science experiments at synchrotron radiation facilities. His two-year visit (2021-2023) at FinEstBeAMS is funded by an Estonian research grant. He participates in user support and has local contact duties at the GPES and SSES.
Jako Siim Eensalu (externally funded postdoc, temporary). Jako has joined the FinEstBeAMS team in September 2022. His ten-month visit at FinEstBeAMS is funded by an Estonian research grant.
In addition, some persons who no longer work at MAX IV have had signification contributions to the construction and development of FinEstBeAMS. Rainer Pärna worked as the project manager of FinEstBeAMS in 2012-2016 – he was responsible for the construction of the FinEstBeAMS beamline – and as the beamline manager in 2016-2019. Vladimir Pankratov worked as a scientist at FinEstBeAMS

in 2016-2019 and was responsible for the construction and commissioning of the PLES. Rami Sankari was the principal designer of the beamline optics.

6.6. Organization of beamline work

Planning for work in a new semester begins when a proposal call closes. The permanent beamline staff have about two weeks to perform a technical feasibility evaluation of the proposals submitted to FinEstBeAMS. Following MAX IV Guideline (Table 6.1), the beamline staff suggest the splitting of the available beamtime between the different categories of use, and, in more detail, how many shifts of beamtime general users should get at each end station. The group manager and the science director will either approve or question that suggestion. The review panels composed of external experts evaluate the scientific merits of the proposals and recommend which of them should be granted with beamtime and with how many shifts. The proposals submitted to FinEstBeAMS are handled in up to four different review panels (LDM, surface science, photoluminenescence, and T&E).

Once the results of the proposals' evaluations have been published, the beamline manager contacts the PIs of the approved proposals. He asks two questions related to the scheduling of the beamtimes: Which weeks are impossible for your experiments? When do you prefer to have your beamtimes scheduled? The beamline manager then makes a draft of the beamtime calendar based on the users' replies and applying some basic boundary conditions. First, we try to minimize the number of exchanges of the experimental setups at Branch A because each exchange causes 1-2 days of extra work to the beamline staff. Second, we try to avoid scheduling more than two consecutive beamtimes at the same end station, so that workload on the same team members would not become excessive. It is not always possible to follow these two conditions if some users have given very few possible time slots for their beamtimes. Our most important criterion for the beamtime calendar is that the general users could actually come to FinEstBeAMS to perform their experiments. In-house research beamtimes are often scheduled in weeks that remained free after the scheduling of the general users' beamtimes. The beamline manager schedules the approved proposals in DUO.

The DUO calendar is not user-friendly to get an overview of what will happen at the beamline. For that purpose, the FinEstBeAMS team use an event calendar in the internet, which can be consulted without a password and to which anybody can insert events. Figure 6.1 shows an example month of that calendar.

The FinEstBeAMS team organize weekly meetings (on Friday mornings), in which we describe how the experiments of the present week are going, go through the tasks of the following week, share information about any events of importance, discuss the results of commissioning work, etc. Every team member is encouraged to speak in these meetings.

The beamline manager writes biweekly reports of the beamline's events for the team's internal use. Those reports may be helpful to find later information about past events because a man's memory is short. Admittedly, the contents of these reports are biased because BM does not know all the details of work that is being done at the SSES and the PLES.

Regarding user operation in practice, local contacts are responsible for interaction with the users who are coming for beamtimes. At the beamline level, there are no general instructions on how this should be done. The solutions differ between the three end stations and have already been described in Sections 3-5.

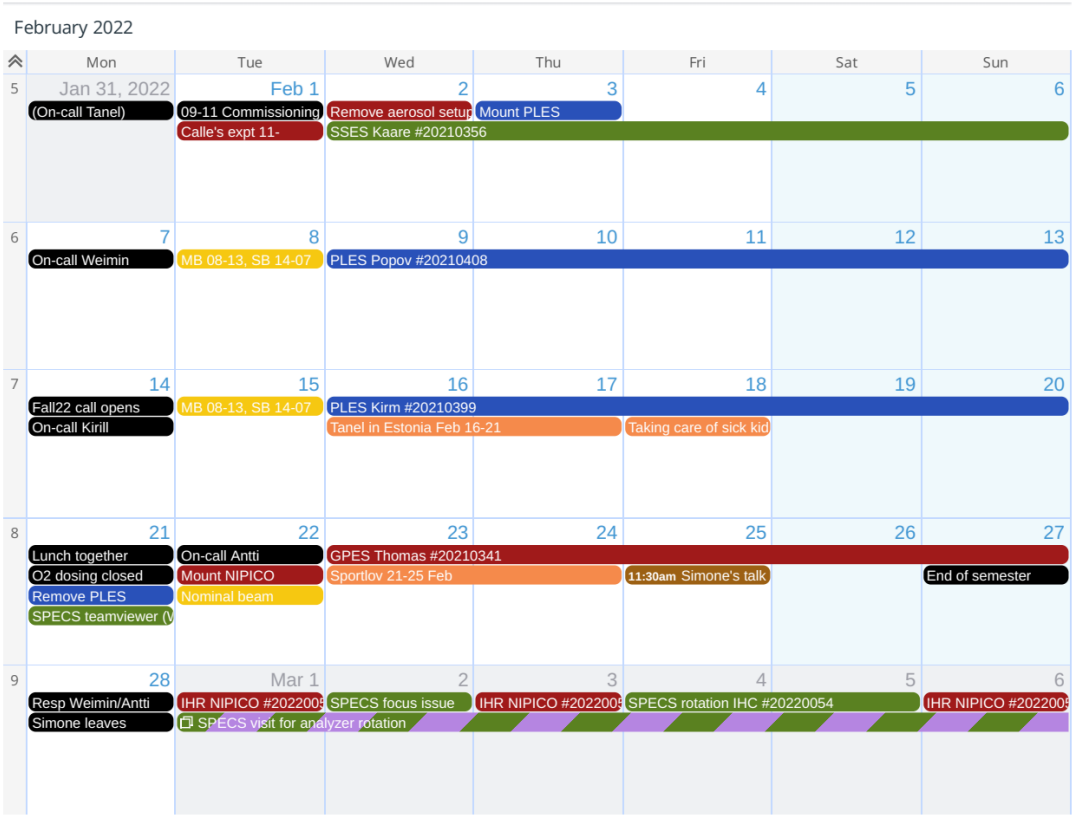

Figure 6.1. *February 2022 in the FinEstBeAMS Event calendar. Events dealing with the GPES are shown in red, those with the PLES in blue, those with the SSES in green, and those with the whole beamline in black. Yellow gives information about the accelerator. Orange is used for absences and leaves.*

6.7. Outreach

The FinEstBeAMS team maintain the FinEstBeAMS web pages at the MAX IV site, where information about the beamline and its end stations are shown. The web pages are updated at the least before each proposal call so that users know about the experimental possibilities at the beamline and what kind of proposals can be submitted. In addition, LDM activities taking place at FinEstBeAMS are reported on the LDM web pages at the MAX IV site.

The FinEstBeAMS team members have participated in scientific meetings and workshops, giving talks and presenting posters about the beamline and its end stations. Doing so at the annual MAX IV User meeting belongs to our natural duties. Outside such meetings, we have not actively visited research groups at universities or research institutes to expand our user community. In 2022, Weimin sent emails to possible users of the SSES in order to attract more proposals. His efforts seemed fruitful. Expanding outreach activities is also a question of manpower. As FinEstBeAMS is understaffed, travels outside MAX IV laboratory pile up other work that should have been done in the meantime.

The FinEstBeAMS team prepare informal newsletters about FinEstBeAMS every three months and send them by email to our closest partners, collaborators and users, as well as to some MAX IV staff members. The newsletters can be used as a channel to spread information about, e.g., status of development projects and new experimental capabilities that have become available to users.

7. User and in-house research

7.1. Molecular fragmentation studies at the Gas-phase end station

A user research example by Edwin Kukk (University of Turku, Finland)

The GPES was designed as a versatile and modular end station suitable for a wide range of gas phase and other non-UHV targets [1]. It is permanently equipped with a hemispherical Scienta R4000 electron analyzer, refitted with a fast electron detector suitable for for coincidence spectroscopy. The other permanent equipment of the GPES is a modified Wiley-McLaren type ion TOF spectrometer, capable of 3D ion momentum imaging and multi-ion coincident detection [1]. These spectrometers can be operated individually or as a combined coincidence system for two-paricle PEPICO, or multi-particle PEPI…PICO experiments.

As with all designs, the GPES coincidence set-up is a result of a compromise, optimized for specific strengths. Compared to various other synchtrotron-based coinicdence setups, the GPES is capable of high electron resolution over a broad kinetic energy range (although maximizing the resolution comes at the cost of acquisition time), combined with a fair ion TOF and momentum resolution, and with a multi-ion simultaneous detection. The system is thus especially well suited for experiments relating the electronic structure properties at the onset of the molecular dynamics (or that of a larger system) to the eventual outcome of the fragmentation processes. Furthermore, the momentum imaging allows to reconstruct the various intermediate stages of the dynamics. The two examples presented here demonstrate the utilization of these properties of the GPES coincidence setup; there are many other types of studies that can be performed with the setup.

7.1.1. Observing electronic decay processes in molecular fragments vs. parent molecule with the help of Doppler effect

An external expert beamtime was carried out by M. Simon's group (CNRS; Soleil) who evaluated GPES's performance in a demanding application combining high electron resolution with momentum imaging. In that experiment [2], vibrationally-resolved resonant Auger spectra of ammonia were recorded in coincidence with the NH_2^+ fragment, which is produced in the course of dissociation of a core-excited state. Correlation of the NH_2^+ ion flight times with electron kinetic energies in a PEPICO map (Fig. 7.1) allows direct observation of the Auger-Doppler dispersion for each vibrational state of the fragment. In addition, distribution of the kinetic energy release E_{KER}, derived from the 3D ion momenta in the coincidence data, revealed new relationships in how and to which extent the available energy (from the Auger electron's energy) is converted into the kinetic energy of the molecular fragments [2].

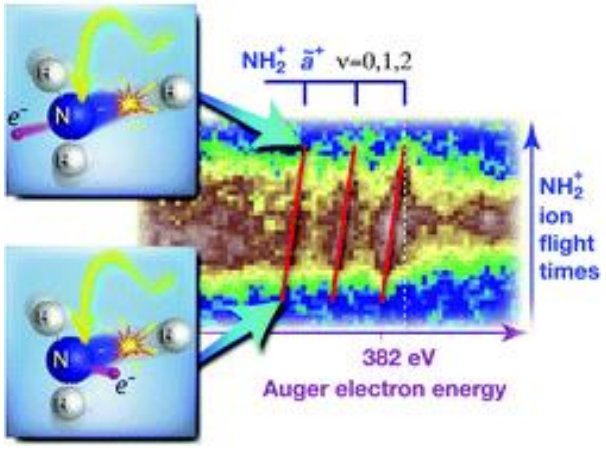

Figure 7.1. *Detail of the electron-ion coincidence (PEPICO) map from the Auger decay of core-excited ammonia. The map shows linear dispersion of the Auger emission energy, a signature that it originates from the NH_2^+ fragment [2].*

Figure 7.1 illustrates the Doppler effect in the Auger emission, by showing a linear dispersion of the electron's energy with the fragment ion's flight time. Shorter flight times correspond to ions moving

away from the electron emission direction and a red-shift in the electron energy. Longer flight times correspond to blue-shift. Red lines in Fig. 7.1 are obtained from a first-principles calculation for the vibrationally resolved Auger spectrum and convincingly confirm the assignment of this part of the spectrum to the Auger emission ***after*** the dissociation [2].
According to the external expert group, the measurement highlighted the particular strengths of the GPES as such results could not be obtained using, e.g. the coincidence setup at Pleiades, Soleil.

7.1.2. Reconstructing the early stages of the radiation damage and fragmentation dynamics by x-ray absorption: diiodothiophene as a showcase

Halogenated organic and biomolecules have attracted considerable interest in recent years [3,4]. Iodine substitutions, for example, can make the molecules absorption "hotspots" and the first stops in the chain of radiation damage. The study reported here – an energy-resolved Auger electron-multiion coincidence measurement of diiodothiophene at the GPES end station – is a showcase of intricate and complex early dynamics with very clean spectroscopic signatures.
The molecular dynamicsin this case is initiated by soft x-ray absortion in I 4d subshell. We determined the internal energy of the parent $C_4SH_2I_2^{++}$ dication, available for moelcualr dissociationm by coincident measurement of the Auger electron's kinetic energy (as these are complementary quantities). The amount of the internal energy available at the onset of dynamics plays a key role in determining its outcome, but can also have a major effect, in the orders of magnitude, on ***how fast*** the dynamics evolves [5].
Probing the time-scale of x-ray dynamics typically requires pump-probe experiments at XFELs, where combining it with high resolution electron spectroscopy is a major challenge. Here we demonstrated a reconstruction of the time-scale of the events along the molecular dynamics pathway using a single photon (non-pump-probe) electron-energy-resolved spectroscopy at a synchrotron facility. As an example, the strongest fragmentation pattern after I 4d ionization produces three fragments: $C_4SH_2^+$, I^+ and neutral I, and the two ions were detected in coincidence with the Auger electron. The slope of the corresponding pattern in the ion-ion coincidence (PIPICO) map of Fig. 7.1 is determined by the sharing of momenta between fragments in a process

$C_4SH_2I_2^{++} \rightarrow C_4SH_2I^+ + I^+ (\tau) \rightarrow C_4SH_2^+ + I + I^+$.

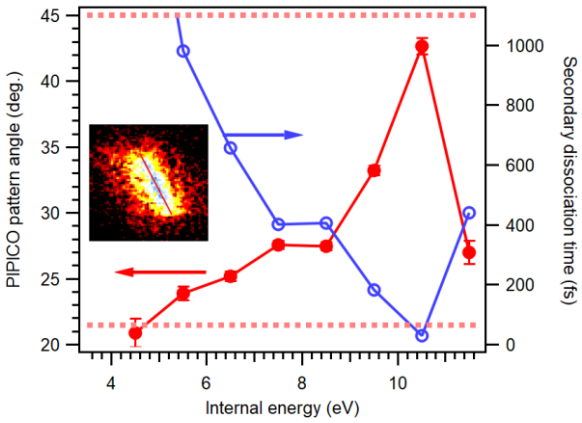

Figure 7.2. *PIPICO pattern's slope and secondary dissociation time τ of the main 3-body process in $C_4SH_2I_2^{++}$.*

By utilizing the electron energy resolution across the detected energy window of about 20 eV, we studied the PIPICO pattern of this process for different internal energy ranges at the onset of the dynamics. The experiment revealed how the slope is a function of the internal energy and from it we can reconstruct the timescale τ of the secondary dissociation event (Fig. 7.2). The data are complemented with the 3D momentum correlation plot using the momentum imaging of the TOF spectrometer.
The dynamics is thus not described as concerted or secondary dissociation, but spans the whole range between the two as an "extended secondary dissociation" model. In terms of the evolution and spread of radiation damage, the timescale of the processes in the original "hotspot" can be a very important factor. The study demonstrates how non-time-resolved spectroscopic methods can efficiently access this information.

*1. K. Kooser et al., J. Synchrotron Rad **27**, 1080 (2020).*
2. O. Travnikova et al., Phys. Chem. Chem. Phys. **24**, 5842 (2022).
*3. L. Pihlava et al., Phys. Chem. Chem. Phys. **23**, 21249 (2021).*

4. F. Allum et al., Faraday Discuss. **228**, 571 (2021).
5. E. Kukk et al., Phys. Rev. Research ***3****, 013221 (2021).*

7.2. Results from the Photoluminescence End Station (PLES)

A user research example by Marco Kirm (University of Tartu, Estonia)

The PLES was successfully launched in its initial configuration at the FinEstBeAMS beamline in 2018 and its capacity has been further developed over years. It has been designed for high quality luminescence spectroscopy under VUV-to-XUV excitation [1]. The heart of the end station is a closed-cycle helium cryostat operating in the temperature range 10 – 350 K. It is attached to the UHV chamber and equipped with an adjustable (X-Y-Z directions) sample holder suitable for mounting more than 40 samples on it. The luminescence from the sample is collected and led out by an optical fiber of 0.3 m length, which is an atypical solution for luminescence experiments. Another longer fiber (~ 2 m) directs collected luminescence to an Andor Shamrock (SR-303i) 0.3 m analyzing spectrometer equipped with three diffraction gratings blazed at 300, 500 and 1200 nm. A set of various detectors (several PMTs, a CCD camera) covers the full operation range of the analyzing spectrometer from 200 to 1350 nm. In a single bunch operation mode of the storage ring, a time-resolved multiphoton counting method, providing 160-200 ps time resolution, was implemented in autumn 2019. The challenges of luminescence studies, largely posed by a grazing incidence geometry of the primary monochromator, are related to the suppression of higher excitation orders by a set of various filters and to distinguishing "white X-ray" disturbances in the measured spectra. The photon flux at FinEstBeAMS is considerably higher (~100 times at the same spectral resolution) than at earlier dedicated luminescence spectroscopy stations. Thus, the measurement conditions are considerably improved, but one has to account for possible sample damage by high-intensity radiation. In summary, PLES has achieved design goals and now serves as an advanced research tool for the whole luminescence community in Europe. Since its launching 2018, more than 20 related papers have been published in leading international journals. Until autumn 2021, PLES at FinEstBeAMS was practically the only synchrotron station in operation for luminescence research in Europe. A dedicated luminescence setup at the P66 NIM beamline on the bending magnet source (PETRA III, DESY) has also been functioning for a year by now. The technical performance of both beamlines with their PLES is complimentary, *e.g.,* P66 widens spectral range in luminescence analysis into the VUV region of 6-10 eV.

7.2.1. Time-integrated photoluminescence of Ce doped garnet scintillators

Cerium doped complex garnets are promising materials for scintillator and persistent phosphor applications. Khanin *et al.* dedicated their study to the identification of the reasons of luminescence efficiency variation in Ce^{3+}- and Ce^{4+}-doped garnets. For this purpose, energy conversion processes were investigated in complex $LuGd_2Ga_3Al_2O_{12}$:Ce^{3+}/Ce^{4+} ceramics by means of VUV synchrotron radiation [2]. Firstly, it was shown by XANES spectroscopy at Balder that codoping of the studied garnets with Mg^{2+} ions results in the formation of Ce^{4+} ions only. Thereafter, FinEstBeAMS PLES was applied for a detailed comparative study of energy transfer processes between intrinsic excitons, Gd^{3+} and Ce^{3+} centers in the samples with different Ce^{3+} and Ce^{4+} content. It was shown that, in a regular scintillator case, there is an efficient energy transfer from excitons through Gd^{3+} ions to Ce^{3+} centers providing an efficient emission at 550 nm. When all Ce^{3+} were converted to Ce^{4+} ions by Mg^{2+} doping of the same host, the excitation spectrum of cerium emission showed no Gd^{3+} f-f or excitonic transitions. Thus, the exciton → Gd^{3+} → Ce^{3+} energy transfer path was interrupted, which was the main reason for a weakened Ce^{3+} luminescence under X-ray excitation of the studied $LuGd_2Ga_3Al_2O_{12}$:Ce, Mg ceramics. This is a perfect example how a high-quality time-integrated luminescence spectroscopy performed in a wide energy (4.5-45 eV) and temperature (7-300 K) ranges can be used in the

identification of very complex energy transfer mechanisms and contribute to the development of advanced scintillators with improved light yield.

7.2.2. Time-resolved photoluminescence research on ternary fluorides with ultrafast emissions

Time-resolved luminescence spectroscopy was implemented owing to a single bunch operation mode, which became available at the 1.5 GeV ring, to a further development of FinEstBeAMS measurement electronics and related software. Because of an undulator used as a radiation source at the FinEstBeAMS, the amount of scattered radiation in the excitation channel is rather small, and this circumstance really facilitates the research of weak and fast (subnanosecond time range) emissions. Such research was performed by Saaring *et al.* for ternary fluorides in order to demonstrate that a complex valence band structure introduces additional ultrafast emissions and to study their excitation mechanisms [3,4]. The developed time-resolved multiphoton counting technique allows the detection of several non-overlapping photons with the time resolution of 160 ps in a single bunch mode (320 ns interval). The advanced software allows convenient recording of a luminescence decay curve at each excitation energy or emission wavelength resulting in time resolved excitation or emission spectra, respectively [4]. The post-experiment analysis of such data allows successful elucidation of relaxation processes of electronic excitations that can lead to the appearance of ultrafast emissions in wide gap materials.

As an example, Fig. 7.3 shows a comparison of the calculated band structure (left panel) and the fast luminescence spectra (detected within the first 3 ns, right panel) revealed experimentally in a $BaGeF_6$ powder [3]. Boxes in the right panel indicate the radiative transitions (i-vi) with the relevant onset energy (a minimal calculated energy distance between the bands involved, shown by arrows in the left panel) and their width (a target band energy width). The electronic structure of the $BaGeF_6$ filled shells comprises the hybridized F 2p and Ge 4s, 4p states positioned in a way, which results in a multiple sub-band structure of the valence band, and the Ba 5p core band state. Thus, a rich luminescence spectrum (right panel) due to various kinds of radiative transitions (intraband and cross-luminescence) is obtained in the compounds with complex valence bands. The peculiarities of relaxation processes of electronic excitations in $BaGeF_6$ as well as in K_2GeF_6 were also analyzed on the basis of the recorded time-resolved excitation spectra and luminescence decay kinetics. The published time-resolved luminescence research clearly demonstrates a power of such experimental method in the development and design of materials with specific properties for scintillation applications. This is also marked by significant interest of researchers from different countries towards the advanced FinEstBeAMS facility.

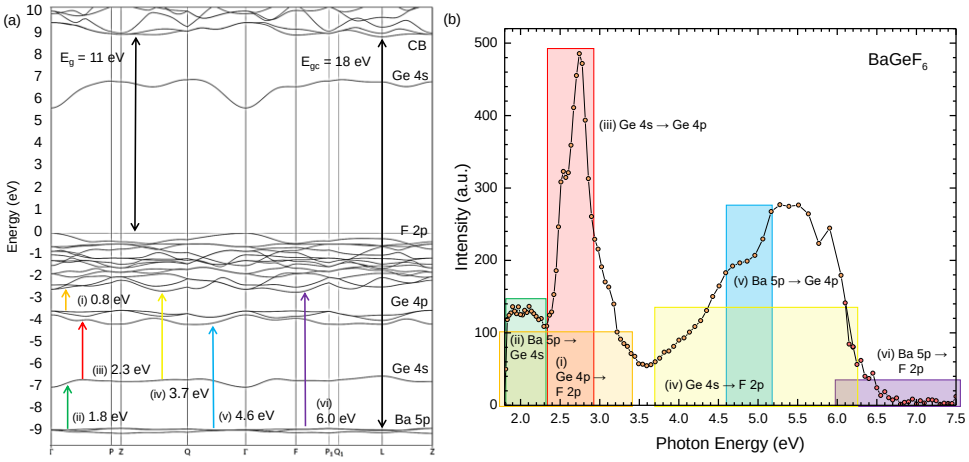

Figure 7.3. *(a) The calculated band structure of $BaGeF_6$. (b) Fast luminescence spectra (detected within the first 3 ns, right panel) measured of $BaGeF_6$ powder.*

1. V. Pankratov *et al.,* Radiation Measurements **121** (2019) 91-98.
2. V. Khanin *et al.,* J. Luminescence **237** (2021) 118150.
3. J. Saaring *et al.*, J. Luminescence **244** (2022) 118729.
4. J. Saaring *et al.*, J. Alloys Compd. **883** (2021) 160916.

7.3. Guanine molecule electronic fingerprint via graphene nanoribbon edge functionalization

An in-house research example by Amirreza Ghassami. This is a modified version of the research example that was included in the original FinEstBeAMS beamline review report.

The research goal here is the on-surface functionalization of the graphene nanoribbons' edges for applications in molecular sensing and as bandgap tuning for carrier transport interlayers. Scanning Probe Microscopy (SPM) tip-based molecular manipulation makes it possible to achieve a specific molecular interaction with a particular direction on a molecule-by-molecule basis. The electronic tunability of graphene nanoribbons made them a promising material for creating molecular fingerprints. We doped 7-AGNR (armchair graphene nanoribbons with seven atom width) with DNA nucleobases. Here the impact of doping on the electronic structure of the 7-AGNR has been studied using scanning tunneling microscopy/spectroscopy (STM/STS) measurements. STM/STS indicated band shifts and molecular bonding mechanisms in various temperatures. PES measurements provided evidence for the molecular bonding mechanism, validated our molecular model, and provided input structure for DFT calculations. Doping 7AGNR edge with guanine molecules reduces the bandwidth of the nanoribbon and introduces impurity levels resulting from the oxygen electron lone pairs. Our density functional theory calculations and scanning tunneling spectroscopy have demonstrated that adding guanine to the 7-AGNR structure reduces its bandgap as the GNR's π-network is extended. Furthermore, we have shown that guanine behaves as n-dopants, significantly downshifting the ribbon bands and introducing deep impurity levels associated with the so-called guanine's oxygen electron lone pairs.

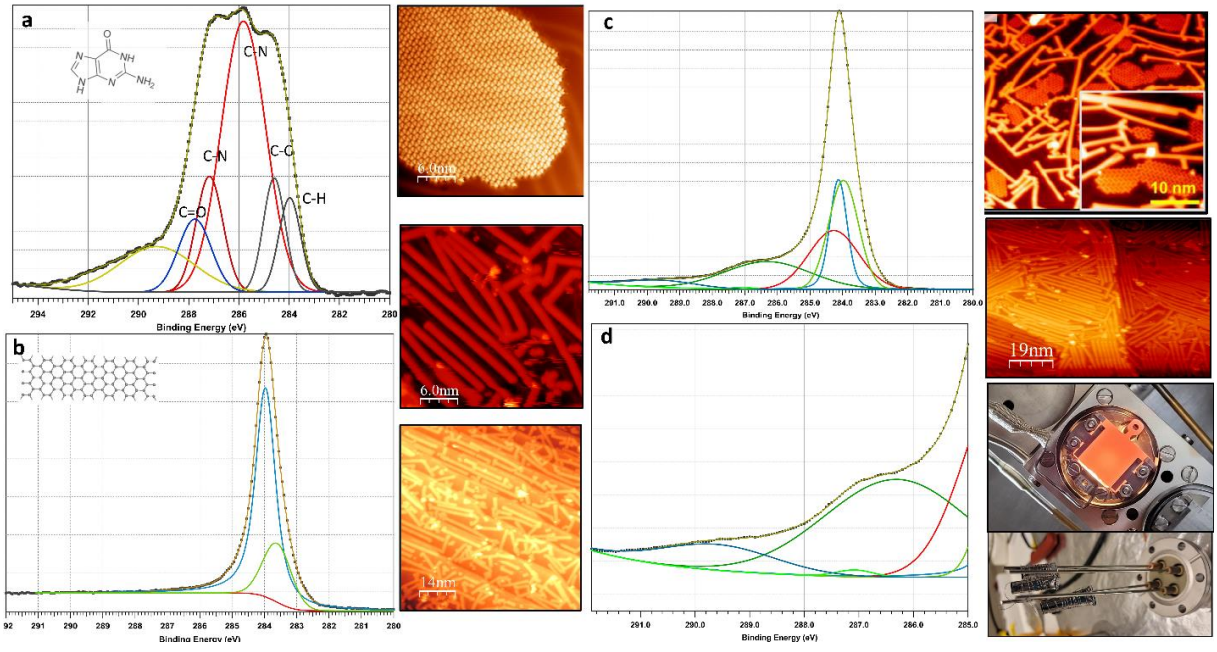

Figure 7.4. *(a) C 1s XPS spectra of (a) Guanine molecules, (b) pristine 7-AGNR, and (c,d) doped 7-AGNR with Guanine 9H molecules on Au(111) surface. After the surface temperature increases to 550 K, the guanine*

molecules without any chemical bonds with the surface or with GNR edges were desorbed from the surface. (b) The spectra show peaks of C-C at 284.3 eV and C-H at 283.7 eV. In (c), XPS spectra of GNRs with guanine molecules show that even after the structure is annealed at 690 K, in which only GNR could remain at the surface, there are guanine molecules at the surface which are chemically bonded with GNRs. (d) A new peak at 290 eV (G-doped 7-AGNR) only appeared after guanine was introduced during GNR synthesis (polymerization). STM image of 7-AGNR on Au(111) surface, and Guanine surface assemblies on Au(111) and Guanine doped GNRs are shown. The handmade triplet evaporation source is used in the perp chamber for the experiments at SSES.

7.4. Aerosol sample delivery system

An in-house research example by Calle Preger. This is a modified version of the research example that was included in the original FinEstBeAMS beamline review report.

Aerosol science and technology is a wide research field which has a large impact on society. Aerosol science includes atmospheric research, air pollution in indoor and workplace environments, emissions from transportation and energy production, design of engineered particles for novel materials, and a range of other applications. An aerosol is a two-phase system with particles suspended in a gas, typically air, and usually at atmospheric pressure. The particle size ranges from a few nm to several microns and can have different shape and composition. Aerosols are complex multi-dimensional systems, and the reactions and dynamics occurs with the particles suspended in the gas. It is therefore important to analyze properly the particles without prior particle collection onto a support. Online, or in-flight, characterization methods are therefore a priority in aerosol research.

A dedicated aerosol sample delivery system (ASDS) at MAX-lab has been a desire for the aerosol research community. Recently, researchers from LTH (Jenny Rissler and Axel Eriksson) and MAX IV (Noelle Walsh and Antti Kivimäki) gathered to realize such a system. Funding was attained from LTH to hire a 2-year postdoc (Calle Preger) and additionally 250 kSEK from Crafoord Stiftelsen was awarded for equipment. In June 2022, a milestone of the project was reached with the first successful beamtime. The next beamtime for commissioning will take place in mid-October 2022. In the spring 2023 term, the system will be open for expert commissioning, and the goal is to have the system accessible for regular users in the fall 2023 proposal call.

The ASDS brings aerosols generated at atmospheric pressure to vacuum in a continuous flow for x-ray photoelectron spectroscopy (XPS) studies. The ASDS is commissioned at FinEstBeAMS but is designed so that it can be mounted at other beamlines. A challenge to perform online XPS studies on aerosols is to bring the aerosol from atmospheric pressure to vacuum without diluting the particle jet. This is achieved by using an aerodynamic lens (*Aerodyne PM1*), which collimates the aerosol particles in a sequence of orifices. After the exit of the aerodynamic lens, the particles enter the source chamber where a large 2150 l/s turbo pump maintains the pressure at ~$1 \cdot 10^{-3}$ mbar. The ASDS is designed to operate with a differential pumping arrangement (using one or two skimmers) equipped with three HiPace80 turbo pumps (Figure 7.5). The pressure in the gas phase end station (GPES) at FinEstBeAMS reaches low 10^{-7} mbar with the aerosol jet running when operating with two skimmers with 1 mm opening. With only one skimmer, the pressure in the GPES is in the low 10^{-6} mbar range.

The first successful experiments using the ASDS were performed by aerosolizing different sea salt particles of atmospheric relevance from a solution (NaCl, $(NH_4)_2SO_4$, Na_2SO_4, NH_4Cl, and mixtures of these). In all cases, the main components could be properly characterized. Carbon and silicon were also measured to ensure low level of particle contamination originating from the tubes and generation. A small carbon signal was observed, but the signal was weak compared to the signal from the salt components.

An advantage of in-flight aerosol characterization using XPS is the possibility to study the components in the particles and surrounding the gas molecules simultaneously. The binding energy of the Cl 2p

component in the gas molecules is shifted by a few eV compared to the particle signal and the characteristic 2p features can therefore easily be resolved in the same energy window.

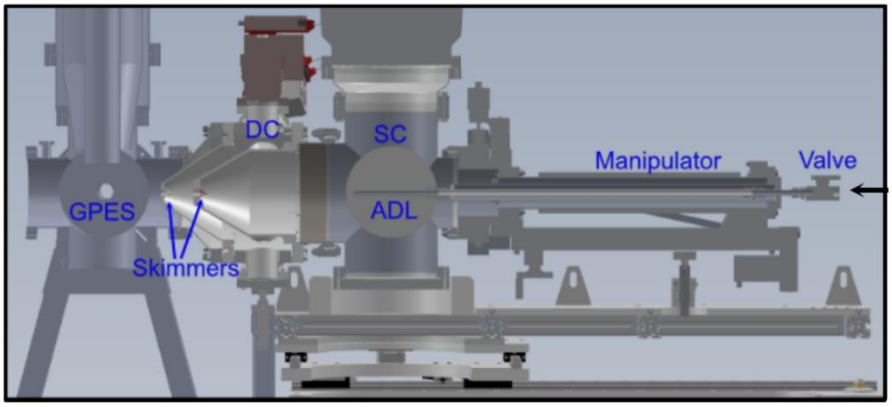

Figure 7.5. *(a) The ASDS mounted at FinEstBeAMS. The aerosol is generated before it enters the ASDS. An XYZ-manipulator holds the aerodynamic lens (ADL) inside the Source chamber (SC). A differential pumping chamber (DC) separates the SC to the gas phase end station (GPES) at FinEstBeAMS and the chambers are separated by two skimmers.*

These are the first results from the new ASDS that has been commissioned at FinEstBeAMS. They show the potential of measuring particle signal from a wide range of particle sizes and number concentration. It also demonstrates the possibilities of measuring the gas and particle signal simultaneously.

7.5. Other in-house research and commissioning

FinEstBeAMS staff members have had several other in-house research beamtimes, in addition to the examples given above. The purposes of these beamtimes can be divided into two main categories. First, we have invited external researchers and performed experiments with them and usually of their interest during in-house research beamtimes. Collaborators can also send their samples to FinEstBeAMS, and the beamline staff members perform the experiments. Second, we have used in-house beamtime to commission or characterize instrumentation. (At the beginning of 2022, a new category of beamtime was established for the latter use of beamtime: in-house commissioning.) The permanent FinEstBeAMS staff members do not pursue their own research topics very actively due to their other duties at the beamline. We have performed some experiments of our own, but presently it is very difficult to find sufficient time for data analysis and writing manuscripts.
The list below gives some examples of in-house research and commissioning beamtimes that we have executed at FinEstBeAMS:

- Proposal 20190638: "Nanoscale solvation of KCl and RbBr in clusters in polar solvents". Outcome: the publication of article No. 9. (GPES; Antti)
- Proposal 20200035: "Commissioning of a negative-ion/positive-ion coincidence instrument". Outcome: NIPICO experiments can be performed at FinEstBeAMS with the available ion TOF spectrometers, electronics and software. See section 3.1.3. (GPES; Antti & Kirill)
- Proposal 20200673: "Commissioning of time-resolved photoluminescence setup and VUV spectroscopy of nonstoichiometric spinel". Outcome: Time-resolved photoluminescence experiments can be performed in single-bunch and multi-bunch modes using the beamline's own instrumentation. (PLES; Kirill)

- Proposal 20200839: "F-type luminescence spectroscopy as a diagnostic tool of the material tolerance to irradiation". Outcome: the publication of article No. 38. (PLES; Kirill)
- Proposal 20200607: "Vacuum annealing induced effects on ALD grown TiO2 (30 nm) thin films supported on Si(100)" and Proposal 20200017: "Temperature-dependent PES experiments of Cu/TiO2". Outcome: The results were used in the article No. 39. (SSES; Weimin)
- Proposal 20220054: "Commissioning of the SPECS analyzer after its rotation". Outcome: Performance of the electron analyser was verified after a major hardware change and before the users' beamtimes. (SSES; Weimin, Tanel & Amirreza)

8. Beamline development

8.1. Universal mode & polarimeter

As the radiation propagates through the beamline, its polarization can change as the reflections on optical elements change the ratio between vertical and horizontal components of the electric field vector and introduce additional phase shift between them. The magnitude of the shift increases with decrease of photon energy and the incidence angle at optics. While changes in ratio between vertical and horizontal components of the electric field vector can be compensated by shifting the magnets in the corresponding EPU mode, the phase shift cannot be compensated therefore at low energies polarization state becomes elliptical in considerable degree (see Fig 2.3).

In order to provide "clean" polarization state at any energy, two tasks have to be completed. First, a new EPU movement mode, which will combine helical and incline modes and allow to change phase shift ratio between vertical and horizontal components of the electric field vector, have to be commissioned. Second, a polarimeter have to be installed that can characterize the polarization state at the endstations in order to find required EPU parameters.

The new undulator movement mode, so-called universal mode, is in the process of commissioning. Control software of the EPU was updated to implement this mode. The polarization of the EPU radiation for different EPU parameters and transmission function of the beamline were calculated to determine initial phase space of the EPU parameters. The obtained phase space need to be verified with a polarimeter. The polarimeter, which has been used for initial commissioning, requires dismounting of an end station to be installed due to its size and has mechanical issues that limit its accuracy, therefore a new, compact polarimeter is needed. As there is no commercially available one, a polarimeter that can stay permanently in an end station was constructed at Bloch beamline, which is also implementing universal mode for their undulator. The polarimeter has common two-stage design, consisting of retarder and analyzer stages. We suggest design based on the Bloch's one, but it will only include the analyzer stage. Having only one stage will allow to simplify alignment and dramatically reduce measurements time, as well as decrease the size and reduce cost of the polarimeter. The drawback of such design is inability to estimate overall degree of polarization (S_0 Stokes coefficient). Considering that degree of polarization is not the parameter that can be affected, it seems to be justifiable to choose the simpler design.

A polarimeter construction project is estimated to take about 6 months and cost around 300 000 SEK.

8.2. Chopper

FinEstBeAMS has received funding for the construction and installation of an optical chopper in the beamline. Carl Tryggers Foundation awarded a grant of 610.5 kSEK for this purpose. That is not enough alone, but the project has become possible with additional funding from the University of Oulu (20 k€) and MAX IV (900 kSEK or 90 k€). The FinEstBeAMS chopper project was approved by the MAX IV Central Project Office, which guarantees that the services of MAX IV resource groups can be used to realize it. The project was launched in March 2022.

The separation of light pulses is 320 ns when the 1.5 GeV ring operates in single-bunch mode. This is not long enough for all time-resolved experiments. In particular, the flight times of electrons in a magnetic bottle electron spectrometer can be several μs, which typically mixes electrons originating from different light pulses (the problem can be partially overcome by exploiting coincidence detection). The chopper will extend the time interval between incident light pulses in single-bunch mode. This is achieved by installing a fast-rotating disk with narrow slits on its outer edge in the path of synchrotron radiation.

The FlexPES beamline already has a chopper. Our main idea has been to install at FinEstBeAMS a chopper that would be quite similar (but not identical) to the one at FlexPES, taking advantage of the

existing design and experiences gained so far at FlexPES. Therefore, Gunnar Öhrwall and Noelle Walsh have actively participated in the FinEstBeAMS chopper project.
A designer from the MAX IV mechanical design group has completed the CAD drawing of the chopper's vacuum chamber, support, and necessary modifications to the FinEstBeAMS beamline. (The latter will not be very extensive.) The customized vacuum parts have been ordered in summer 2022.
Stefan Plogmaker finished the design of the chopper disc in May 2022. There will be 120 similar, laser-cut slits on the outer edge of the chopper disc. The length and width of the slits will be 3 mm and ~85 μm, respectively. The thickness of the disc at the outer edge could be either 0.8 or 1.2 mm. Stefan recommended the acquisition of the thicker disc because it could withstand better strain caused by rapid rotation of the disc. The rotation will be synchronized to the ring clock of the storage ring. The maximum frequency would be ~1000 Hz, whereby every 27th light pulse in single-bunch mode could pass through a slit in the chopper and lead to 8.64 μs intervals in the chopped photon beam.
The head of the MAX IV mechanical design team advised that one company should be responsible for both the production of the disc and laser-cutting of the slits. This narrowed our search to a company that also delivered the chopper disc for FlexPES. The company has not yet sent us quotations of the production of two different chopper discs, but according to preliminary information the production of the disc would only be possible in spring 2023.
When the thickness of the disc has been chosen, procurement of the motor and balancing of the chopper disk can be started with the help of the MAX IV procurement office. That will be the most expensive part of the chopper project.

8.3. Continuous scanning

Measurements of excitation spectra at PLES and NEXAFS at SSES require scanning of photon energy. Acquisition time in these measurements is relatively short and comparable with the moving time of the monochromator and the EPU, which results in significant amount of moving dead time, up to 70%. To eliminate this dead time, it is proposed to commission the control system to work in continuous scanning mode, where data would be acquired while the monochromator and the undulator continuously change photon energy with some constant speed.
Linear scanning of photon energy results in non-linear speeds in monochromator and undulator motors. So-called parametric trajectories that perform such movements were already implemented for the monochromator at FlexPES beamline, so the implementation can be utilized at FinEstBeAMS. Implementation of parametric trajectories for the undulator movement remain to be a task in development. Currently, constant speed of the EPU gap is used as an easy approximation, which works well for relatively short scans.
Continuous scanning will require hardware synchronization. Control electronics will be based on the PandAbox, which has been already acquired. Cable installations has to be done. Substantial work will be needed to configure all detectors to run with external synchronization. It is expected to take about three months for equipment installation and commissioning of EPU and monochromator movement.

8.4. Prioritization of the development projects

Resources to large and medium-size development projects are coordinated at the laboratory level. This means that a beamline cannot begin a project at its own will, but it must be accepted by the CPO (large projects) or by the MAX IV management (medium-size and small PBAG projects). Furthermore, funding to cover the costs of the project must be approved. An overview of the development projects for FinEstBeAMS that are in progress or planned for the near future is presented in Table 8.1. Projects marked as "Active" do not need further funding or another trigger to proceed. We have divided the

other projects in three categories according to our opinion: high, medium and low priority. We have given high priority to such projects that will benefit many experiments and will not require excessive funding or resources to be realized. We would like to ask the review panel whether they endorse our prioritization. If not, which projects are the most important ones for the development of FinEstBeAMS?

Table 8.1. *Overview of ongoing and planned development projects at FinEstBeAMS.*

Project (discussed on page)	End station/ Beamline	Required resources and estimated duration	Status
Active			
Gas handling system (p. 21)	GPES	CPO-coordinated project (across several beam-lines), resources are secured	Restart in fall 2022
Chopper (p. 60)	Beamline	CPO-approved project, resources are secured	In progress
Integration of Scienta and SPECS control software (p. 20)	GPES, SSES	CPO-coordinated project, resources are secured	In progress
High priority			
Continuous scanning (p. 61)	Beamline	Electronics unit (Panda-box) has been acquired. KITS Software, KITS Hardware, electricians	Waiting for MAX IV decision
Universal mode & polarimeter (p. 60)	Beamline	EPU has been upgraded. KITS Software, KITS Hardware, SAM, Design office, Mechanical workshop Polarimeter is not funded (estimate 300 kSEK), ~6 months for construction, then commissioning	Waiting for funding
Diagnostic chamber (p. 34)	SSES	Design ready, not funded (estimate 146 kSEK)	Waiting for funding
Medium priority			
Installation of Al-coated grating (p. 13)	Beamline	In collaboration with Tartu Uni. Procurement of grating blanks is starting.	future plans
Redesign of M1 chamber (p. 12)	Beamline	Waiting to see results from other beamlines.	future plans
Integration of the QMS control software (p. 35)	SSES		future plans
UV lamp installation (p. 40)	SSES	Tartu Uni will acquire a lamp for FinEstBeAMS.	In progress
XRF detector installation (p. 40)	SSES		future plans
Low priority			
Extra prototype of receiver (p. 35)	SSES		future plans
“Dirty” preparation chamber (p. 41)	SSES		future plans